IDENTIFYING BUILDING LOCATIONS
IN THE WILDLAND-URBAN
INTERFACE WITH CONVOLUTIONAL
NEURAL NETWORKS

by

Neda K. Kasraee

A thesis submitted in partial fulfillment of

the requirements for the degree of

Master of Science

(Forestry)

at the

UNIVERSITY OF WISCONSIN-MADISON

2022

Advisor Approval Page

APPROVED

Volker Radeloff

Professor

08/26/2022

Acknowledgments

First, I would like to thank my advisor Volker Radeloff for his support and guidance. I am grateful for the opportunity to think critically while being nudged in the right direction when needed. I leave graduate school with improved technical skills and as a better writer and researcher. I would also like to thank Todd Hawbaker for providing great suggestions for my first chapter, which helped me think beyond the scope of my initial project. I would like to thank Mutlu Ozdogan for helping me improve my remote sensing skills in his class. Additionally, I would like to thank Volker, Todd, and Mutlu for being on my committee and providing feedback that helped improve my research.

Next, I would like to thank my family – my mom, dad, sisters Naseem and Parveen, and dogs Tom and Jerry. My family has instilled in me a work ethic I am proud of and taught me how to be kind and hardworking, all things that served me well in graduate school and life. I would also like to thank my husband Dan for his continued support and for encouraging me to take opportunities to advance my career, even if that means being far apart.

Lastly, I would like to thank everyone in the SILVIS lab for enriching my graduate school experience.

Abstract

Buildings in the wildland-urban interface (WUI) are especially at-risk of destruction during wildfire seasons, but despite these risks, the WUI has grown over the last several decades. WUI maps are not frequently updated due to the lack of available data, especially pre-1990s. For my first chapter, my goal was to apply convolutional neural networks (CNNs) to extract building data from imagery and estimate building destruction post-wildfire. Specifically, I looked at three California fires: Camp, Tubbs, and Woolsey. Since CNNs are technically complex and challenging for non-computer scientists to apply, I evaluated a CNN-based building dataset from Microsoft and a pre-trained CNN model from Esri to detect buildings from high-resolution imagery. I found moderate accuracies for both the Microsoft dataset and the Esri CNN model. Occluding vegetation caused underestimation of buildings and their destruction rates in densely forested areas. The Esri CNN model had post-fire accuracies of ≥ 73%, suggesting that CNNs can be used with moderate accuracies for post-fire building identification. However, while CNNs can be used to determine if an area is WUI or not-WUI, they are not accurate enough for reliable building counts. For my second chapter, I utilized historical spy satellite data from the Hexagon program to extract building and land cover information to map the WUI for the 1970s. Again, I used CNNs to extract building locations, and I used an object-oriented classification to extract land cover data. I selected two study areas, one in Southern California, US, and one in New South Wales, Australia. To observe WUI change, I compared my 1970s WUI maps to current WUI maps. I used the Microsoft building footprint dataset (updated in the late 2010s, early 2020s) and for land cover, I used the National Land Cover Database for the US study area and the European Space Agency

WorldCover dataset (updated 2020) for the Australia study area. For the US study area, the WUI covered 49% in 1973 and for the Australia study area, the WUI covered just 6% in 1976. However, the WUI grew by 7 percentage points from 1973 to the present-day for the US study area, and the WUI grew by 34 percentage points from 1976 to the present-day for the Australia study area. My final WUI maps had an overall high accuracy. We visually inspected 100 randomly placed circular sample areas and in the samples we visually inspected, 94 of the 100 samples had the correct WUI classification, and all 100 samples had the correct WUI classification for the Australia study area. I found that the historical spy satellite Hexagon provides valuable land cover and building information and can be used to map the WUI accurately for the 1970s. Both my chapters show the limitations and benefits of CNNs for building identification, and I also provide a method for extracting land cover and building data from historical spy satellite imagery to study long-term WUI growth.

Introduction

The WUI, the area where the built environment intermixes or intermingles with wildland vegetation, is a central location for land management issues. For example, the WUI disproportionally experiences human-caused ignitions which consequently threatens residential homes (Keeley and Fotheringham, 2003; Syphard et al., 2007; Mietkiewicz et al., 2020) because houses are in close proximity to fuels (Syphard et al., 2004, Kramer et al., 2009). Aside from wildfire risks, the WUI and its growth is also a central location for the introduction and spread of invasive species, habitat fragmentation and loss, and pollution from nearby settlements and roads (Bar-Massada et al., 2014). Despite the various risks associated with the WUI, the WUI continues to grow and in the US, it was the fastest growing land use type from 2000-2010 (Radeloff et al., 2018).

The WUI and the associated consequences with its growth is a global problem, and WUI maps are developed in many countries for risk assessments and identifying communities with high wildfire risk, especially during wildfire seasons. For example, WUI maps have been created and used by the European Union (Modugno et al., 2016), the US (Radeloff et al., 2018), Central Argentina (Argañaraz et al., 2017), and Poland (Kaim et al., 2018).

With the continued growth of the WUI, it is valuable to have up-to-date WUI maps. Unfortunately, WUI maps are difficult to update frequently because building data is not frequently updated. Additionally, it is difficult to go back in time and map the WUI to assess long-term WUI growth, especially pre-1990s, when high-resolution satellite imagery and historical aerial photographs were limited. In the US, WUI maps are created using US Census Data but Census data is released only every 10 years, is not available prior to 1990 at the block level, and too coarse for building-level information as information is provided for a statistical area or “census block” (Radeloff et al., 2018). Additionally, in the US, WUI maps have also been created using building-level data from Microsoft, but Microsoft only releases building footprints for one period of time so updates are not possible (Bar-Massada, 2021; Carlson et al., 2022). In Central Argentina, a WUI map was created by hand digitizing 276,700 buildings (Argañaraz et al., 2017), but that is very labor intensive. However, new remote sensing methods may provide a more efficient method for mapping and updating the WUI. Specifically, I explored the feasibility of applying convolutional neural networks (CNNs) and spatial data to extract building information. CNNs have been used for large-area classifications (Postadjian et al., 2017) such as for disaster response (Dong et al., 2021; Zheng et al., 2021) and land cover mapping (Li et al., 2022; Wambugu et al., 2021).

Although CNNs are powerful, they are demanding to use, as they require large, diverse training datasets and technical sophistication of users. However, existing CNN-derived building datasets and pre-trained CNN models that extract building information are available (Zhu et al., 2017), which raises the question of how accurate they are.

First Chapter: CNN evaluation chapter

For my first chapter, I evaluated an existing CNN-based building dataset and an existing CNN model to identify building locations pre- and post-wildfire and to assess building destruction. I specifically looked at three fire perimeters in California: Woolsey, Tubbs, and Camp fires. I used Microsoft’s nationwide building footprint dataset. The Microsoft building footprint dataset is derived from high-resolution satellite data, a semantic segmentation algorithm, and ResNet34 with RefineNet up-sampling layers (Microsoft, 2018). The

Microsoft building dataset has been used with generally high accuracy for WUI mapping (Bar-Massada, 2021; Carlson et al., 2022). Additionally, I used a pre-trained CNN model from Esri, the Building Footprint Extraction – USA model.

My first chapter research questions were: (1) Can the Esri CNN model detect buildings in the WUI as well as or better than the Microsoft building dataset? (2) Does the Esri CNN model correctly detect intact buildings pre- and post-fire and correctly not detect destroyed buildings post-fire? (3) Do building characteristics and vegetation density influence building detection and destruction rates?

I found that the Microsoft building dataset and the Esri CNN model had low to moderate accuracies, and neither performed better than the other did. When evaluating the accuracy for detecting buildings post-fire, the Microsoft building dataset had accuracies of 48% for the Camp Fire, 60% for the Tubbs Fire, and 58% for the Woolsey Fire. The Esri CNN model had accuracies of 74% for the Camp Fire, 29% for the Tubbs Fire, and 58% for the Woolsey Fire. The Esri CNN model performed well in areas without dense vegetation, and the model sometimes missed minor buildings such as detached garages and mobile homes. The model performed generally well when looking at major buildings only with < 50% tree cover and it performed best in the interface WUI where there was less tree cover than in the intermix WUI. In the interface WUI, the pre- and post-fire CNN model overall accuracy for major buildings with < 50% tree cover was 76% for the Camp Fire, 86% for the Tubbs Fire, and 72% for the Woolsey Fire. Densely forested areas of all three fires had very low accuracy.

However, I also found that the CNN model severely underestimated total buildings and subsequently underestimated total building destruction post-wildfire. The model underestimated building destruction by 33-66% for all three fires (41% total). During my accuracy assessment, I found that although the resulting maps had generally low commission errors (≤ 4%), omission errors ranged between 5-58% with the intermix WUI having more omission errors than the interface WUI. However, I did find that the CNN model produced high enough accuracies to detect WUI versus not-WUI, as did the Microsoft building dataset (Bar-Massada, 2021; Carlson et al., 2022). A building density threshold (6.17 units/km^2) is used for WUI mapping, which allows for some error. As long as the threshold is met, and it often is in urban areas, the WUI will correctly be detected. Ultimately, my first chapter results found that CNNs performed best in areas with sparse vegetation and although CNNs perform well enough to detect WUI vs not-WUI, results should be interpreted with caution when evaluating building counts or assessing building destruction.

Second Chapter: Hexagon WUI mapping chapter

The WUI has grown globally. Unfortunately, it is difficult to study long-term WUI growth because WUI maps do not date before the 1990s since building and land cover data are not available for the past, especially pre-1980s when 30 m Landsat became available. However, high-resolution spy satellite imagery from the Hexagon program is available and may be used to create WUI maps for the 1970s. In my first chapter, I learned that CNNs perform with high enough accuracies to detect WUI and not-WUI areas. For my second chapter, I wanted to expand on the use of CNNs and extract building information from Hexagon imagery for my study areas in Southern California, US, and New South Wales, Australia.

Observing patterns of growth and reduction in the WUI in different regions of the world may provide examples of successful or unsuccessful land use practices for mitigating wildfire risk. Additionally, I used an object-oriented approach to extract land cover data from Hexagon. To study WUI change in the last half-century, we also created current WUI maps using the Microsoft building footprint dataset (updated in the late 2010s, early 2020s), and for land cover, we used the European Space Agency WorldCover (updated 2020) dataset for the Australia study area and the National Land Cover Database (updated 2019) dataset for the US study area.

My second chapter research questions were: (1) Can I use historical satellite imagery from Hexagon to extract building data with CNNs and land cover data with an object-oriented classification approach to accurately map the WUI? (2) Has there been WUI growth or reduction in my study areas, and if so, what are the major reasons for WUI change?

In my second chapter, I found during the accuracy assessment that the final WUI maps had an overall accuracy of 94% for the US study area and 100% for the Australia study area. The object-oriented classification for deriving land cover was moderately accurate. The US study area had an overall accuracy of 80±3% and the Australia study area had an overall accuracy of 77±4%. I found that there was sometimes confusion between agriculture and wildland vegetation but this only affected the WUI maps for the US study area. For the US WUI maps, the 6% that was not correct was solely due to the misclassification of agriculture as wildland vegetation. This caused some areas to be defined as intermix WUI instead of interface WUI. However, those areas were still correctly defined as the WUI. Additionally, I found that the

WUI grew by 7 percentage points from 1973 to the present-day in the US study area, and the WUI grew by 34 percentage points from 1976 to the present-day in the Australia study area.

I found the CNN model had low to moderate accuracies at detecting buildings, and the threshold for defining areas as WUI or not-WUI allowed for some building detection errors. The US study area CNN model had an overall accuracy of 80% with 2% commission errors and 20% omission errors. For the Australia study area, the CNN model had an overall accuracy of 60% with 36% commission errors and 40% omission errors. Overall, I found that the CNN model was accurate enough to detect the WUI vs not-WUI, and the CNN model did not cause a false WUI classification in any instance. Ultimately, my results demonstrate that CNNs and object-oriented classification methods perform well enough to map the WUI with high accuracy. My second chapter results also highlights the value of using historical spy satellite imagery, especially for studying the WUI, and other long-term land use change processes.

References

Argañaraz, J.P., Radeloff, V.C., Bar-Massada, A., Gavier-Pizarro, G.I., Scavuzzo, C.M., Bellis, L.M., 2017. Assessing wildfire exposure in the Wildland-Urban Interface area of the mountains of central Argentina. J. Environ. Manage. 196, 499–510.

Bar-Massada, A., 2021. A Comparative Analysis of Two Major Approaches for Mapping the Wildland-Urban Interface: A Case Study in California. Land. 10, 679.

Bar-Massada, A., Radeloff, V.C., Stewart, S.I., 2014. Biotic and Abiotic Effects of Human Settlements in the Wildland–Urban Interface. BioScience. 64, 429–437.

Carlson, A.R., Helmers, D.P., Hawbaker, T.J., Mockrin, M.H., Radeloff, V.C., 2022. The wildland-urban interface in the United States based on 125 million building locations. Ecol. Appl. e2597.

Dong, Z., Wang, G., Amankwah, S.O.Y., Wei, X., Hu, Y., Feng, A., 2021. Monitoring the summer flooding in the Poyang Lake area of China in 2020 based on Sentinel-1 data and multiple convolutional neural networks. Int. J. Appl. Earth Obs. Geoinf. 102, 102400.

Kaim, D., Radeloff, V.C., Szwagrzyk, M., Dobosz, M., Ostafin, K., 2018. Long-Term Changes of the Wildland–Urban Interface in the Polish Carpathians. ISPRS Int. J. Geo-Inf. 7, 137

Keeley, J.E., Fotheringham, C.J., 2003. Impact of past, present, and future fire regimes on North American Mediterranean shrublands, in: Veblen, T.T., Baker, W.L., Montenegro, G., Swetnam, T.W. (Eds.), Fire and Climatic Change in Temperate Ecosystems of the Western Americas, Ecological Studies. Springer-Verlag, New York, pp. 218-262.

Kramer, H., Mockrin, M., Alexandre, P., Radeloff, V., 2019. High wildfire damage in interface communities in California. Int. J. Wildland Fire 28, 641-650.

Li, J., Zhang, B., Huang, X., 2022. A hierarchical category structure based convolutional recurrent neural network (HCS-ConvRNN) for Land-Cover classification using dense MODIS Time-Series data. Int. J. Appl. Earth Obs. Geoinf. 108, 102744.

Microsoft, 2018. US Building Footprints. https://github.com/microsoft/USBuildingFootprints/ (accessed 21 April 2022).

Mietkiewicz, N., Balch, J.K, Schoennagel, T., Leyk, S., Denis, L.A., Bradley, B.A., 2020. In the Line of Fire: Consequences of Human-Ignited Wildfires to Homes in the U.S. (1992–2015). Fire. 3, 50.

Modugno, S., Balzter, H., Cole, B., Borrelli, P., 2016. Mapping regional patterns of large forest fires in Wildland–Urban Interface areas in Europe. J. Environ. Manage. 172, 112–126.

Postadjian, T., Le Bris, A., Sahbi, H., Mallet, C., 2017. Investigating the Potential of Deep Neural Networks for Large-Scale Classification of Very High Resolution Satellite Images. ISPRS Ann. Photogramm. Remote Sens. Spatial Inf. Sci. IV-1/W1, 183–190.

Radeloff, V.C., Helmers, D.P., Kramer, H.A., Mockrin, M.H., Alexandre, P.M., Bar-Massada, A., Butsic, V., Hawbaker, T.J., Martinuzzi, S., Syphard, A.D., Stewart, S.I., 2018. Rapid growth of the US wildland-urban interface raises wildfire risk. PNAS 115, 3314–3319.

Syphard, A.D., Brennan, T.J., Keeley, J.E., Syphard, A.D., Brennan, T.J., Keeley, J.E., 2014. The role of defensible space for residential structure protection during wildfires. Int. J. Wildland Fire. 23, 1165–1175.

Syphard, A.D., Radeloff, V.C., Keeley, J.E., Hawbaker, T.J., Clayton, M.K., Stewart, S.I., Hammer, R.B., 2007. Human Influence on California Fire Regimes. Ecol. Appl. 17, 1388–1402.

Wambugu, N., Chen, Y., Xiao, Z., Wei, M., Aminu Bello, S., Marcato Junior, J., Li, J., 2021. A hybrid deep convolutional neural network for accurate land cover classification. Int. J. Appl. Earth Obs. Geoinf. 103, 102515.

Zheng, Z., Zhong, Y., Wang, J., Ma, A., Zhang, L., 2021. Building damage assessment for rapid disaster response with a deep object-based semantic change detection framework: From natural disasters to man-made disasters. Remote Sens. Environ. 265, 112636.

Zhu, X.X., Tuia, D., Mou, L., Xia, G.S., Zhang, L., Xu, F., Fraundorfer, F., 2017. Deep learning in remote sensing: A comprehensive review and list of resources. *IEEE Geosci. Remote Sens. Mag. 5,* 8-36.

Table of Contents

List of Figures

List of Tables

List of Appendices

Chapter 1: Identifying building locations in the wildland-urban interface before and after fires with convolutional neural networks

Contributors: Neda K. Kasraee[1,*], Todd J. Hawbaker[2], Volker C. Radeloff [1]

[1] SILVIS Lab, Department of Forest and Wildlife Ecology, University of Wisconsin-Madison, 1630 Linden Drive, Madison WI 53706, USA.

[2] U.S. Geological Survey, Geosciences and Environmental Change Science Center, Denver, CO 80225, USA, ORCID: 0000-0003-0930-9154

Abstract

Wildland-urban interface (WUI) maps identify areas with wildfire risk, but they are often not updated frequently due to the lack of building data. Convolutional neural networks (CNNs) can extract building locations from remote sensing data, but their accuracy in WUI areas is unknown. Additionally, CNNs are computationally intensive and technically complex making it challenging for end users, such as those who use or create WUI maps, to apply. Our aim was to map buildings pre- and post-wildfire and estimate building destruction for three California wildfires: Camp, Tubbs, and Woolsey. We did this by evaluating and utilizing a CNN-based building dataset from Microsoft and a CNN model from Esri to detect buildings from high-resolution satellite imagery. This dataset and model represent to end users the state-of-the-art of what is readily available for potential WUI mapping. We found only moderate accuracies for the Microsoft dataset and the Esri CNN model and a severe underestimation of buildings and their destruction rates where trees occluded buildings. The Esri CNN model performed best post-fire with accuracies ≥ 73%. Existing CNNs may be used with moderate accuracy for identifying individual buildings post-fire and mapping the extent of the WUI. However, CNNs are not accurate enough for post-fire damage assessments or building counts in the WUI.

Keywords

Housing growth, urbanization, wildland fire, wildfire hazard, machine learning, aerial photography, building detection, wildfire destruction

Introduction

Wildfires largely affect communities in the wildland-urban interface (WUI), the area where buildings intermix or intermingle with wildland vegetation. In the U.S., housing in the WUI has grown rapidly since 1990 (Keeley et al., 1999; Radeloff et al., 2018), and increasingly severe wildfire seasons have resulted in record-setting destruction of homes (Cruz et al., 2012; Kramer et al., 2019; Tedim et al., 2020). Although wildfires are a natural phenomenon, climate change, human ignitions, and alteration of fuels have changed historical fire regimes (Bowman et al., 2009; Chuvieco et al., 2014; Marlon et al., 2009). On the one hand, fire suppression has reduced fire frequency in many areas, especially the frequency of lower-intensity surface fires (Agee and Skinner, 2005; Smith et al., 2022; Syphard et al., 2007). On the other hand, wildfires have been introduced to ecosystems not accustomed to them (Chuvieco et al., 2014), and in some areas, there has been an increase in fire severity and frequency compared to historical fire regimes (Bowman et al., 2009; Chuvieco et al., 2014). More frequent wildfires have many far-reaching ecological and socioeconomic impacts, including the increased risk of building destruction.

WUI maps are useful for risk assessments and identifying communities that experience high wildfire risk. The WUI has been mapped for many regions including Central Argentina (Argañaraz et al., 2017), the European Union (Modugno et al., 2016), Lebanon (Mhawej et al., 2017), and the United States (Radeloff et al., 2018). Some drivers of WUI growth include recreational amenities (Godoy et al., 2019), forest regrowth (Kaim et al., 2018), and, generally, new developments as people move towards more rural areas adjacent to or within wildland vegetation (Hammer et al., 2009). In the future, the WUI is likely to continue growing as people seek access to natural amenities and ecosystem services (Radeloff et al., 2018). WUI growth has several negative environmental effects, such as habitat loss, introduction and spread of invasive species, pollutants from nearby settlements and roads, and wildfire ignition (Bar-Massada et al., 2014).

Unfortunately, WUI maps are challenging to update frequently. WUI maps require two inputs – wildland vegetation data and building data. The latter is the most difficult to acquire since most building datasets are not updated frequently enough to account for increased urbanization. In the United States, housing density data is available from the U.S. Census, but Census data is only available every decade (Radeloff et al., 2018, 2005; Stewart et al., 2007). Furthermore, WUI maps that use Census data are often too coarse for building-level analysis and risk assessments (Carlson et al., 2022), and do not capture where buildings were destroyed by wildfires. However, new remote sensing methods derived from algorithms for object or image recognition may allow for mapping the WUI with finer spatial resolution and for efficient updates to WUI maps (Bar-Massada, 2021). Specifically, convolutional neural networks (CNNs) and spatial data can be applied for large-area classifications (Postadjian et al., 2017). CNNs have been utilized for various remote sensing applications such as disaster response (Dong et al., 2021; Zheng et al., 2021) and land cover mapping (Li et al., 2022; Wambugu et al., 2021). CNNs utilize spectral and spatial properties as they relate to each other, unlike pixel-based classifications, which use only spectral information. As such, CNNs are efficient, especially when compared to hand digitizing objects (Brodrick et al., 2019).

While CNNs are very powerful, they are also fairly demanding in terms of computing power, size of training datasets, and technical sophistication of users. Particularly, the creation of a customized CNN model from scratch is challenging for a non-computer scientist because it is not clear which CNN structure will detect buildings best (Kattenborn et al., 2021). Additionally, CNNs require a large, diverse training dataset, which often is not available, and resources may limit training dataset collection (Song et al., 2019). However, there are both existing CNN-derived building datasets and pre-trained CNN models (Zhu et al., 2017) which represent for many end users the state-of-the-art datasets or models that they can use, raising the question of how accurate either are.

An excellent example of the power of CNNs to map objects for large areas is Microsoft's nationwide building footprint dataset. The Microsoft building dataset is derived from high-resolution satellite data. In the United States, the reported overall classification accuracies of the Microsoft building footprints are 98.5% precision and 92.4% recall (Microsoft, 2018). The Microsoft building dataset has been used for WUI mapping with generally high accuracy in California (Bar-Massada, 2021) and across the United States (Carlson et al., 2022). We selected this dataset because it is the premier broad-scale building dataset derived from CNNs that is available. The Microsoft dataset was the first to provide building locations at a continental scale when it was initially released in 2015, and the U.S. has been continuously updated since. Furthermore, Microsoft is now providing similar data for most of Africa and Europe, and Google has also released a comparable CNN-based building dataset for Africa.

We focus on building detection in the WUI because of a) the importance of the WUI for wildfire management and b) the challenges when identifying buildings in the WUI given the density and proximity of vegetation. Overhanging trees may occlude buildings and affect the accuracy of building footprints produced by either hand digitization or image classifications

(Bittner et al., 2018; Hoeser and Kuenzer, 2020; Kramer et al., 2019). Vegetation cover is most likely in the intermix WUI, potentially causing a bias when assessing destruction in the interface versus the intermix WUI. However, CNNs may detect buildings near vegetation that pixel-based methods may have missed. It is not clear what the accuracy of the Microsoft building dataset is where trees occlude buildings.

An alternative to the analysis of existing CNN-derived building datasets is to apply existing CNN models to pre- and post-fire remote sensing imagery. One example of a pre-trained CNN model is the Building Footprint Extraction – USA model by Environmental Systems Research Institute (Esri). The Esri CNN model can be applied to multi-band high-resolution imagery to extract building locations, and Esri reported that the average precision score is 71.8% (Esri, 2021). An advantage of using the Esri CNN model is that it has customizable parameters and can be implemented in any study area where high-resolution imagery is available. However, the reported accuracies appear to mainly represent the results in urban areas, where most buildings are located, and it is not clear what the accuracy is in areas with dense vegetation cover such as the WUI. We selected this model because, like the Microsoft data, it is the most accessible to end users. Esri is globally a leading GIS software program, and many natural resource management agencies are already using Esri software to manage their spatial data. Documentation and default parameters make this model easier to use than other available CNN models because it can be applied without modifications or training data, but permits tuning to local conditions.

In summary, our goal was to examine how accurately both existing CNN-based building datasets and existing CNN models can identify building locations pre- and post-wildfire and estimate building destruction. To meet this goal, we evaluated the accuracy of CNNs for building detection in the WUI as available in (a) an existing dataset, from Microsoft, and (b) an existing CNN model, from Esri for three destructive California wildfires: Camp, Tubbs, and Woolsey. Specifically, we had three research questions: (1) Can the Esri CNN model detect buildings in the WUI as well as or better than the Microsoft building dataset? (2) Does the Esri CNN model correctly detect intact buildings pre- and post-fire and correctly not detect destroyed buildings post-fire? (3) Do building characteristics and vegetation density influence building detection and destruction rates? We expect that the Esri CNN model and Microsoft building dataset would have similar accuracies and that CNNs would detect building pre-fire and post-fire overall well, but with lower accuracy in the intermix WUI due to occluding vegetation. Ultimately, we aim to demonstrate to end users the benefits and drawbacks of utilizing CNNs for WUI mapping and post-fire damage assessment via either a readily available building dataset or a pre-trained CNN model.

Methods

Study area

California is an ideal study area to assess whether CNNs provide accurate results for building identification before and after fires due to its long history of destructive, deadly, and costly wildfires. Most of California is fire-prone with fuel-dominated and wind-dominated fires, and its Mediterranean-climate shrublands are a fuel source that can drive high-intensity fires when ignited (Keeley et al., 1999; Keeley and Syphard, 2019). Fire suppression and increased anthropogenic ignitions have altered California fire regimes, resulting in increased fire frequency (Keeley and Fotheringham, 2003) and suppression cost. In California, wildfires have led to increased total structure damage over the last four decades (Buechi et al., 2021). In the 2020 California fire season alone, there were nearly 10,000 fires, which resulted in about 1.74 million hectares burned, 33 fatalities, and 10,500 buildings that were damaged or destroyed (CAL FIRE, 2021). The 2020 California fire season also marked the first "gigafire" when the August Complex Fire burned about 418,000 hectares (1,033,000 acres).

We analyzed three wildfires: Camp, Tubbs, and Woolsey (Figure 1). These three fires are among the top ten most destructive wildfires in California's history (CAL FIRE, 2021). The Camp Fire is California's most destructive and deadliest wildfire, burning 62,242 hectares, destroying 18,804 buildings, and killing 85 people. The Tubbs Fire burned 14,895 hectares, destroyed 5,636 structures, and killed 22 people while the Woolsey Fire burned 39,233 hectares, destroyed 1,643 structures, and killed three people.

Data

The California Department of Forestry and Fire (CAL FIRE) collects data on unaffected, damaged, and destroyed buildings to assess the extent of wildfire damage. Through the California Public Records Act, we accessed this ground collected damage dataset, which we refer to as the CAL FIRE ground-truth dataset, to assess building loss for the Camp, Tubbs, and Woolsey Fires. Damage is classified as: No Damage, Affected (1-9% of the building damaged), Minor (10-25%), Major (26-50%), and Destroyed (> 50%). In all three fires, we found that buildings classified as > 50% destroyed were completely burned down. We used the CAL FIRE ground-truth dataset to verify the results from the Esri CNN Model and

Microsoft building dataset. We also obtained fire perimeters from CAL FIRE for the Camp Fire, Tubbs Fire, and Woolsey Fire (CAL FIRE FRAP).

To assess whether CNN accuracy differed by WUI type, we used an independent WUI classification based on the 2010 United States Census data to identify intermix and interface WUI (Radeloff et al., 2018). Within the three fire perimeters, about 27% was in the intermix WUI and 4% was in the interface WUI. The other 68% was uninhabited or did not have enough wildland vegetation to qualify as WUI.

The Microsoft United States building footprint dataset, first released in 2018, contains 129,591,852 building footprints (as of April 2022) derived from Bing Imagery and a CNN semantic segmentation algorithm (Microsoft, 2018). Microsoft applied Deep Neural Networks and ResNet34 with RefineNet up-sampling layers to detect buildings from Bing imagery (Microsoft, 2018). The Microsoft building dataset was the first dataset to demonstrate that CNNs can map building footprints at a national scale and was only in 2021 surpassed in size by Google's Africa-wide building footprint dataset (Sirko et al., 2021).

Creating Buildings Footprints with the Esri CNN Model

We also created our own building footprint dataset pre- and post-fire with the Esri CNN model. The Esri CNN model uses a Mask Region-based CNN (Mask R-CNN) architecture to determine the location of intact buildings. The Mask R-CNN architecture creates a high-quality segmentation mask while concurrently detecting objects in the imagery and is simple to train, while highly accurate (He et al., 2018). The Esri CNN model is pre-trained, uses ArcGIS API for Python to implement the Mask R-CNN architecture, and maps polygons for each building (Figure 2).

We applied the Esri CNN model to National Agriculture Imagery Program (NAIP) imagery (Earth Resources Observation and Science Center, 2017). We used NAIP imagery taken before (1.5 years maximum) and after (2 years maximum) each wildfire. NAIP imagery typically has no more than 10% cloud cover per quarter quad tile, and it is acquired during the growing season in the United States. Since 2016, 0.6 m NAIP imagery is acquired every two years in select states. NAIP imagery is typically available with four bands (blue, green, red, and near-infrared), and nadir collections reduce the effects of shadows.

Esri CNN Model Building Footprints and Microsoft Building Footprints

We compared the ability of the Microsoft building dataset and the Esri CNN model to detect post-fire buildings. We selected this model and dataset because they represent state-of-the-art datasets, and are readily available to researchers and resource managers alike. We evaluated the accuracy of both the Microsoft dataset and the Esri CNN model output by using CAL FIRE ground-truth data. We were not able to evaluate the accuracy of the Microsoft building data pre-fire due to differences between the date of the wildfire and the date when the Microsoft building dataset was last updated (Table 1). Since the Microsoft building dataset was sometimes updated before the wildfire, the dataset may have marked destroyed buildings as intact. Thus, a pre-fire comparison was not possible and our evaluation of the Microsoft building dataset was limited to a post-fire comparison. Additionally, we only analyzed buildings from the Esri CNN model that the CAL FIRE ground-truth dataset reported were not affected (0% damage) by the fires. Therefore, there was no concern about whether the Microsoft dataset or Esri CNN model detected a destroyed building or a building that was destroyed and then rebuilt. Lastly, we considered a building as correctly detected if a building footprint at least partially overlapped a building in the NAIP imagery.

Identifying Destroyed and Intact Buildings Pre-Fire and Post-Fire

We applied the Esri CNN model on NAIP imagery to create pre - and post-fire building footprint datasets. We then used the Esri CNN model to estimate where buildings had been destroyed in the intermix and interface WUI. To identify the locations of destroyed buildings, we compared the Esri CNN model building footprints for pre-fire and post-fire. If a building was present pre-fire but absent post-fire, we inferred that the building was destroyed. We used the CAL FIRE ground-truth dataset to verify whether the building had indeed been destroyed.

For each fire's accuracy assessment, we conducted a stratified random sample on our post-classification change detection results (Figure 3). First, we manually examined ≥ 8% of the buildings that the Esri CNN model detected in each fire. We visually inspected every building within the stratified random sample in the NAIP imagery to assess whether the Esri CNN model correctly detected a building pre-fire and post-fire, if that building was not destroyed. If a building was destroyed, we checked to see that the Esri CNN model did not detect a building after the fire, and we used the CAL FIRE ground-truth dataset to verify building destruction. We then calculated the post-classification change detection accuracy for each fire. We also estimated the overall accuracy, errors of commission, and errors of omission for each wildfire, pre-fire and post-fire. Errors of commission reflected how many buildings were detected in locations where no building was present in the NAIP imagery, and errors of omission reflected how many buildings were not detected where a building was actually present in the NAIP imagery.

Factors Affecting CNN Results

We collected additional data during our accuracy assessment such as building type and percent vegetation cover to assess which variables may have influenced CNN accuracy. We also made note of whether there was a presence/absence of a Microsoft footprint and whether a destroyed building was rebuilt. For building type, we documented if a building was major, such as residential or commercial, or minor, such as a shed, utility building, or a detached garage. We verified building type using the CAL FIRE ground-truth dataset. For percent vegetation cover directly overtop a building, we noted if the building had no vegetation cover (< 50%), partial tree cover (< 99%), and full tree cover (100%).

We fit a spatial logistic regression model in R Studio using the spaMM package (RStudio Team; Rousset and Ferdy, 2004) for all the buildings included in our accuracy assessment for the three fires. We modeled the probability of a discrete outcome which was building destruction (destroyed, not destroyed) given our two predictor variables which were tree cover (none, partial, full) and fire (Camp, Tubbs, Woolsey). Since our data is observational and not randomized in space, we checked for spatial autocorrelation in the data by fitting a non-spatial regression model, assuming independence in space, and we plotted the residuals which showed very little evidence of autocorrelation. However, after using Moran's I test for distance-based autocorrelation, we found significant evidence of spatial autocorrelation in the data. Therefore, we fit our spatial logistic regression model considering the spatial dependency in the residuals and assessed the significance of regression coefficients to determine whether overhanging vegetation influenced the likelihood of a building being destroyed.

Results

Post-Fire Building Detection with CNNs

Both the Microsoft building dataset and the Esri CNN post-fire model results had moderate to low overall accuracies for the three fires. Neither dataset performed substantially better than the other. The Microsoft building dataset had a post-fire accuracy of 48% for the Camp Fire, 60% for the Tubbs Fire, and 58% for the Woolsey Fire. The Esri CNN model had a post-fire accuracy of 74% for the Camp Fire, 29% for the Tubbs Fire, and 58% for the Woolsey Fire.

Locations of Buildings and Building Destruction with CNNs

In general, the Esri CNN model performed well in areas without dense vegetation, such as the interface WUI (Table 2). However, we found high rates of omission errors in forested areas due to trees obscuring buildings, especially in the intermix WUI. The accuracy increased for all three fires when examining only major buildings and buildings with < 50% tree cover (Table 2) showing that ideal areas for CNNs were those without dense vegetation near buildings, such as the interface WUI. In the interface WUI, the pre- and post-fire CNN model overall accuracy for major buildings with < 50% tree cover was 76% for the Camp Fire, 86% for the Tubbs Fire, and 72% for the Woolsey Fire. Densely forested areas of all three fires had very low accuracy. Suburban and urban areas had overall higher accuracy than rural areas.

Based on buildings detected by the Esri CNN model, 10,549 buildings were destroyed (6,186, 3,320, and 1,043 in the Camp, Tubbs, and Woolsey fires, respectively). However, the actual number of buildings destroyed in the CAL FIRE ground-truth dataset was 26,024 and hence much higher (18,798, 5,636, and 1,590, respectively), indicating that the Esri CNN model severely underestimated building destruction by 33% to 66% (41% in total).

In our accuracy assessment of the Esri CNN model results, we also calculated errors of commission and errors of omission for each fire, pre- and post-fire (Table 3). Commission errors were generally low (≤ 4%). However, omission errors were large and ranged between 5% and 58%. We found that the intermix WUI had more omission errors than the interface WUI both pre- and post-fire. We also found that errors of omission were higher pre-fire than post-fire. The reason for both was likely due to tree cover in the intermix WUI and before fires occurred. Generally, overall accuracy was higher post-fire, and commission and omission errors were lower because a considerable portion of the tree cover was burned, making buildings more visible.

During our accuracy assessment, we found that rebuilding was minimal as expected since the post-fire imagery used for the Esri CNN model was taken less than 2 years after each fire. For the Camp Fire and Tubbs Fire, only 4% of destroyed buildings were rebuilt while for the Woolsey Fire, 3% of destroyed buildings were rebuilt. For < 2% of buildings, we could not tell if a building was rebuilt due to dense vegetation.

Factors Influencing CNN Accuracy and Building Destruction

Based on our accuracy assessment, several factors influenced the CNN’s ability to detect buildings. Building type influenced CNN accuracy, especially for the Esri CNN model, which missed many minor buildings. The amount of vegetation obscuring a building also affected the accuracy of the CNNs, and buildings with full tree cover were often not detected by both the Esri CNN model and the Microsoft building dataset (Figure 4). Building loss estimates were thus biased due to the influence of vegetation on CNNs, resulting in the under-detection of buildings. Building detection decreased with increased vegetation, and according to our spatial logistic regression model, buildings with full tree cover have a higher likelihood of being destroyed by a wildfire (Table 4). This could further negatively bias building loss estimates because destroyed buildings with full tree cover would not be detected pre-fire or post-fire.

The low accuracy of building detections in forested areas resulted in a strong bias when assessing building destruction in intermix versus interface WUI. Overall, the Esri CNN model underestimated how many buildings were destroyed in the intermix WUI (Figure 5). For the entire study area, the Esri CNN model found that 49% of all destroyed buildings were in the intermix WUI while 50% were in the interface WUI, compared to 56% versus 30% in the CAL FIRE ground-truth dataset. Underestimation in forested areas is concerning because we found that buildings with overhanging vegetation have a higher probability of being destroyed. According to our spatial logistic regression model, among the buildings that the Esri CNN model identified, those with full tree cover had a 95% probability of being destroyed. Buildings with partial tree cover had a 77% lower risk of being destroyed than a building with full tree cover, and buildings with no tree cover had an 88% lower risk of being destroyed than a building with full tree cover. Because the Esri CNN model missed many buildings pre-fire with full tree cover that may have been destroyed, this is a conservative estimate.

Discussion

CNNs offer great promise for mapping building footprints efficiently for large areas and could potentially be used to assess building destruction from wildfires rapidly. Although our results show that existing CNNs applied to high-resolution aerial imagery are not accurate enough for building-level assessments, accuracy is generally high enough to assess whether an area is WUI or not (Bar-Massada, 2021; Carlson et al., 2022). However, accuracy is lower for minor buildings and buildings partially or fully covered by trees, and that creates a bias when estimating how many buildings were destroyed in the interface versus intermix WUI because a larger fraction of buildings in the intermix WUI are missed.

The accuracies from the Esri CNN model and the Microsoft building dataset had substantial variability when mapping buildings post-fire. Although the accuracies varied, both datasets worked well in ideal cases, such as those without dense vegetation near buildings. CNNs applied to these areas may allow for point-based WUI mapping. When creating WUI maps, some omitted buildings still allow for accurate WUI mapping as long as the building density threshold is still met (Carlson et al., 2022). The US Federal Register's definition of the WUI does not include isolated buildings in or near wildland vegetation (USDA and USDI, 2001). Instead, minimum building density thresholds are defined to identify communities, or clusters of buildings. This makes footprint-based WUI maps robust to omission errors, and, the accuracy of the classification into WUI versus non-WUI may still be high, even when the accuracy of the building detection itself is low. However, estimates of the number of buildings in the WUI based on CNNs are likely erroneous, and so would be estimates of building growth in the WUI. Furthermore, there were regional biases in that the Microsoft building dataset included the majority of buildings in some regions, but not in others.

Uneven building detection by CNNs causes a bias when identifying what proportion of buildings are destroyed in intermix versus interface WUI. The reason is that interface WUI had an overall higher accuracy for detecting buildings individually, which means that the pre-fire baseline is more accurate. CNNs may be more beneficial to mapping the interface WUI. For destructive California fires that burned between 1985 to 2013, the interface WUI experienced the greatest total amount of building destruction (Kramer et al., 2019). CNNs can assist in the mapping of some high fire risk areas, such as the interface WUI. However, in intermix WUI, too many pre-fire buildings were missed to provide an accurate estimate of rates of destruction by wildfires.

We found that occluding vegetation and building size limited CNN accuracy both pre- and post-fire. Occlusion by vegetation, and also by shadows, is a common problem for building detection (Khoshboresh-Masouleh et al., 2020). However, when mapping buildings in the WUI, buildings occluded by vegetation are especially important because they have an elevated risk of destruction during wildfires because the vegetation near provides fuel that can potentially ignite buildings (Cohen, 2000; Syphard et al., 2014). For example, in Australia, there is a strong correlation between overhanging vegetation and building destruction from wildfires (Leonard et al., 2009). Similarly, we found that buildings that were fully occluded by vegetation had the highest probability of being destroyed, whereas buildings with no occluding vegetation have the smallest probability of being destroyed.

Limitations

We found several limitations when applying CNNs on aerial imagery. The Esri CNN model requires imagery with < 1 m resolution that is taken at close to nadir. However, the availability of such data was limited for our study area and elsewhere too. We selected NAIP for our study because the imagery has a resolution of 0.6 meters. However, because the NAIP imagery was taken over several days, sun angles differed, and the appearance of shadows was greater in some images. Also, NAIP is available in the United States only, and only during the growing season, which means that trees are fully leafed out. Our study area had little to no deciduous forests, but in study areas with deciduous forests, leaf-off imagery would be preferable. Imagery from other sensors that penetrate tree canopies may be effective for building detection. For example, LIDAR data (Gamal et al., 2020; Griffiths and Boehm, 2019) and synthetic aperture radar data (Fibæk et al., 2021; Xu et al., 2020) have been used with CNNs to extract building information.

Conclusion

CNNs applied to aerial imagery are capable of detecting individual building footprints in areas with low vegetation cover. In such areas, CNNs could provide detailed maps of building locations for wildfire management and mapping the WUI. However, our results indicated that CNNs have lower accuracy where vegetation is dense and where buildings are smaller than a single-family residential home, such as mobile home communities. In these areas, building maps derived from CNNs may be accurate enough to map WUI versus non-WUI, but not accurate enough to estimate building counts or to assess destruction due to wildfires.

References

Agee, J.K., Skinner, C.N., 2005. Basic principles of forest fuel reduction treatments. For. Ecol. Manage. 211, 83–96.

Argañaraz, J.P., Radeloff, V.C., Bar-Massada, A., Gavier-Pizarro, G.I., Scavuzzo, C.M., Bellis, L.M., 2017. Assessing wildfire exposure in the Wildland-Urban Interface area of the mountains of central Argentina. J. Environ. Manage. 196, 499–510.

Bar-Massada, A., 2021. A Comparative Analysis of Two Major Approaches for Mapping the Wildland-Urban Interface: A Case Study in California. Land. 10, 679.

Bar-Massada, A., Radeloff, V.C., Stewart, S.I., 2014. Biotic and Abiotic Effects of Human Settlements in the Wildland–Urban Interface. BioScience. 64, 429–437.

Bittner, K., Adam, F., Cui, S., Körner, M., Reinartz, P., 2018. Building Footprint Extraction From VHR Remote Sensing Images Combined With Normalized DSMs Using Fused Fully Convolutional Networks. IEEE J. Sel. Top. Appl. Earth Obs. Remote Sens. 11, 2615–2629.

Bowman, D.M.J.S., Balch, J.K., Artaxo, P., Bond, W.J., Carlson, J.M., Cochrane, M.A., D'Antonio, C.M., DeFries, R.S., Doyle, J.C., Harrison, S.P., Johnston, F.H., Keeley, J.E., Krawchuk, M.A., Kull, C.A., Marston, J.B., Moritz, M.A., Prentice, I.C., Roos, C.I., Scott, A.C., Swetnam, T.W., Werf, G.R. van der, Pyne, S.J., 2009. Fire in the Earth System. Science 324, 481–484.

Brodrick, P.G., Davies, A.B., Asner, G.P., 2019. Uncovering Ecological Patterns with Convolutional Neural Networks. Trends Ecol. Evol. 34, 734–745.

Buechi, H., Weber, P., Heard, S., Cameron, D., Plantinga, A.J. 2021. Long-Term Trends in Wildfire Damages in California. Int. J. Wildland Fire. 30, 757-67.

CAL FIRE, 2021. Top 20 Most Destructive California Wildfires. https://www.fire.ca.gov/media/t1rdhizr/top20_destruction.pdf. (accessed 25 April 2022).

CAL FIRE FRAP. Fire Perimeters. https://frap.fire.ca.gov/frap-projects/fire-perimeters/ (accessed 18 April 2022).

Carlson, A.R., Helmers, D.P., Hawbaker, T.J., Mockrin, M.H., Radeloff, V.C., 2022. The wildland-urban interface in the United States based on 125 million building locations. Ecol. Appl. e2597.

Chuvieco, E., Martínez, S., Román, M.V., Hantson, S., Pettinari, M.L., 2014. Integration of ecological and socio-economic factors to assess global vulnerability to wildfire. Glob. Ecol. Biogeogr. 23, 245–258.

Cohen, J.D., 2000. Preventing Disaster: Home Ignitability in the Wildland-Urban Interface. J. For. 98, 15–21.

Cruz, M.G., Sullivan, A.L., Gould, J.S., Sims, N.C., Bannister, A.J., Hollis, J.J., Hurley, R.J., 2012. Anatomy of a catastrophic wildfire: The Black Saturday Kilmore East fire in Victoria, Australia. For. Ecol. Manag. 284, 269–285.

Dong, Z., Wang, G., Amankwah, S.O.Y., Wei, X., Hu, Y., Feng, A., 2021. Monitoring the summer flooding in the Poyang Lake area of China in 2020 based on Sentinel-1 data and multiple convolutional neural networks. Int. J. Appl. Earth Obs. Geoinf. 102, 102400.

Earth Resources Observation and Science Center, 2017. National Agriculture Imagery Program.

Esri, 2021. Building Footprint Extraction - USA - Overview. https://www.arcgis.com/home/item.html?id=a6857359a1cd44839781a4f113cd5934/ (accessed 25 April 2022).

Fibæk, C.S., Keßler, C., Arsanjani, J.J., 2021. A multi-sensor approach for characterising human-made structures by estimating area, volume and population based on sentinel data and deep learning. Int. J. Appl. Earth Obs. Geoinf. 105, 102628.

Gamal, A., Wibisono, A., Wicaksono, S.B., Abyan, M.A., Hamid, N., Wisesa, H.A., Jatmiko, W., Ardhianto, R., 2020. Automatic LIDAR building segmentation based on DGCNN and euclidean clustering. J. Big Data. 7, 102.

Godoy, M.M., Martinuzzi, S., Kramer, H.A., Defossé, G.E., Argañaraz, J., Radeloff, V.C., 2019. Rapid WUI growth in a natural amenity-rich region in central-western Patagonia, Argentina. Int. J. Wildland Fire. 28, 473–484.

Griffiths, D., Boehm, J., 2019. Improving public data for building segmentation from Convolutional Neural Networks (CNNs) for fused airborne lidar and image data using active contours. ISPRS J. Photogramm. Remote Sens. 154, 70–83.

Hammer, R.B., Stewart, S.I., Radeloff, V.C., 2009. Demographic Trends, the Wildland–Urban Interface, and Wildfire Management. Soc. Nat. Resour. 22, 777–782.

He, K., Gkioxari, G., Dollár, P., Girshick, R., 2018. Mask R-CNN. arXivLabs, Retrieved 25 April 2022, from the arXiv database.

Hoeser, T., Kuenzer, C., 2020. Object Detection and Image Segmentation with Deep Learning on Earth Observation Data: A Review-Part I: Evolution and Recent Trends. Remote Sens. 12, 1667.

Kaim, D., Radeloff, V.C., Szwagrzyk, M., Dobosz, M., Ostafin, K., 2018. Long-Term Changes of the Wildland–Urban Interface in the Polish Carpathians. ISPRS Int. J. Geo-Inf. 7, 137.

Kattenborn, T., Leitloff, J., Schiefer, F., Hinz, S., 2021. Review of Convolutional Neural Networks (CNN) in vegetation remote sensing. ISPRS J. Photogramm. Remote Sens. 173, 24-49.

Keeley, J.E., Fotheringham, C.J., 2003. Impact of past, present, and future fire regimes on North American Mediterranean shrublands, in: Veblen, T.T., Baker, W.L., Montenegro, G., Swetnam, T.W. (Eds.), Fire and Climatic Change in Temperate

Ecosystems of the Western Americas, Ecological Studies. Springer-Verlag, New York, pp. 218-262.

Keeley, J.E., Fotheringham, C.J., Morais, M., 1999. Reexamining Fire Suppression Impacts on Brushland Fire Regimes. Science 284, 1829–1832.

Keeley, J.E., Syphard, A.D., 2019. Twenty-first century California, USA, wildfires: fuel-dominated vs. wind-dominated fires. Fire Ecol. 15, 24.

Khoshboresh-Masouleh, M., Alidoost, F., Arefi, H., 2020. Multiscale building segmentation based on deep learning for remote sensing RGB images from different sensors. J. Appl. Remote Sens. 14, 1-21.

Kramer, H., Mockrin, M., Alexandre, P., Radeloff, V., 2019. High wildfire damage in interface communities in California. Int. J. Wildland Fire 28, 641-650.

Leonard, J., Blanchi, R., Lipkin, F., Newnham, G., Siggins, A., Opie, K., Culvenor, D., 2009. Bushfire CRC Building and land-use planning research after the 7th February 2009 Victorian bushfires: Preliminary findings. CSIRO and Bushfire CRC.

Li, J., Zhang, B., Huang, X., 2022. A hierarchical category structure based convolutional recurrent neural network (HCS-ConvRNN) for Land-Cover classification using dense MODIS Time-Series data. Int. J. Appl. Earth Obs. Geoinf. 108, 102744.

Marlon, J.R., Bartlein, P.J., Walsh, M.K., Harrison, S.P., Brown, K.J., Edwards, M.E., Higuera, P.E., Power, M.J., Anderson, R.S., Briles, C., Brunelle, A., Carcaillet, C., Daniels, M., Hu, F.S., Lavoie, M., Long, C., Minckley, T., Richard, P.J.H., Scott, A.C., Shafer, D.S., Tinner, W., Umbanhowar, C.E., Whitlock, C., 2009. Wildfire responses to abrupt climate change in North America. PNAS 106, 2519–2524.

Mhawej, M., Faour, G., Adjizian-Gerard, J., 2017. Establishing the Wildland-Urban interface building risk index (WUIBRI): The case study of Beit-Meri. Urban For. Urban Greening. 24, 175–183.

Microsoft, 2018. US Building Footprints. https://github.com/microsoft/USBuildingFootprints/ (accessed 21 April 2022).

Modugno, S., Balzter, H., Cole, B., Borrelli, P., 2016. Mapping regional patterns of large forest fires in Wildland–Urban Interface areas in Europe. J. Environ. Manage. 172, 112–126.

Postadjian, T., Le Bris, A., Sahbi, H., Mallet, C., 2017. Investigating the Potential of Deep Neural Networks for Large-Scale Classification of Very High Resolution Satellite Images. ISPRS Ann. Photogramm. Remote Sens. Spatial Inf. Sci. IV-1/W1, 183–190.

Radeloff, V.C., Hammer, R.B., Stewart, S.I., 2005. Rural and suburban sprawl in the U.S. midwest from 1940 to 2000 in its relation to forest fragmentation. Conserv. Biol. 19, 793-805.

Radeloff, V.C., Helmers, D.P., Kramer, H.A., Mockrin, M.H., Alexandre, P.M., Bar-Massada, A., Butsic, V., Hawbaker, T.J., Martinuzzi, S., Syphard, A.D., Stewart, S.I., 2018. Rapid growth of the US wildland-urban interface raises wildfire risk. PNAS 115, 3314–3319.

Rousset, F., Ferdy, J., 2014. Testing environmental and genetic effects in the presence of spatial autocorrelation. Ecography 37, 781-790.

RStudio Team (2020). RStudio: Integrated Development for R. RStudio, PBC, Boston, MA. http://www.rstudio.com/.

Sirko, W., Kashubin, S., Ritter, M., Annkah, A., Bouchareb, Y.S.E., Dauphin, Y., Keysers, D., Neumann, M., Cisse, M., Quinn, J., 2021. Continental-Scale Building Detection from High Resolution Satellite Imagery. arXivLabs, Retrieved 25 April 2022, from the arXiv database.

Song, J., Gao, S., Zhu, Y., Ma, C., 2019. A survey of remote sensing image classification based on CNNs. Big Earth Data. 3, 232-254.

Smith, H., de Beurs, K.M., Neeson, T.M., 2022. Evaluation of low-resolution remotely sensed datasets for burned area assessment within the wildland-urban interface. Remote Sens. Appl.: Soc. Environ. 26, 100752.

Stewart, S.I., Radeloff, V.C., Hammer, R.B., Hawbaker, T.J., 2007. Defining the Wildland–Urban Interface. J. For. 105, 201–207.

Syphard, A.D., Brennan, T.J., Keeley, J.E., Syphard, A.D., Brennan, T.J., Keeley, J.E., 2014. The role of defensible space for residential structure protection during wildfires. Int. J. Wildland Fire. 23, 1165–1175.

Syphard, A.D., Radeloff, V.C., Keeley, J.E., Hawbaker, T.J., Clayton, M.K., Stewart, S.I., Hammer, R.B., 2007. Human Influence on California Fire Regimes. Ecol. Appl. 17, 1388–1402.

Tedim, F., Leone, V., Coughlan, M., Bouillon, C., Xanthopoulos, G., Royé, D., Correia, F.J.M., Ferreira, C., 2020. 1 - Extreme wildfire events: The definition, in: Tedim, F., Leone, V., McGee, T.K. (Eds.), Extreme Wildfire Events and Disasters. Elsevier, pp. 3–29.

USDA, USDI, 2001. Urban wildland interface communities within vicinity of federal lands that are at high risk from wildfire. Fed Regist. 66, 751–777.

Wambugu, N., Chen, Y., Xiao, Z., Wei, M., Aminu Bello, S., Marcato Junior, J., Li, J., 2021. A hybrid deep convolutional neural network for accurate land cover classification. Int. J. Appl. Earth Obs. Geoinf. 103, 102515.

Xu, X., Lu, Y., Zou, B., 2020. Building Extraction From PolSAR Image Based on Deep CNN with Polarimetric Features, in: 2020 21st International Radar Symposium (IRS). Presented at the 2020 21st International Radar Symposium (IRS), pp. 117–120.

Zheng, Z., Zhong, Y., Wang, J., Ma, A., Zhang, L., 2021. Building damage assessment for rapid disaster response with a deep object-based semantic change detection framework: From natural disasters to man-made disasters. Remote Sens. Environ. 265, 112636.

Zhu, X.X., Tuia, D., Mou, L., Xia, G.S., Zhang, L., Xu, F., Fraundorfer, F., 2017. Deep learning in remote sensing: A comprehensive review and list of resources. IEEE Geosci. Remote Sens. Mag. 5, 8-36.

Table 1: Acquisition dates

Dates of National Agricultural Imagery Program (NAIP) acquisition, fire dates, and Microsoft building footprint acquisition.

	Date of Fire (Started – Contained)	Dates of NAIP Acquisition – Pre Fire	Dates of NAIP Acquisition – Post Fire	Dates of Microsoft Building Acquisition
Camp Fire	2018/11/08 - 25	2018/07/16 2018/07/18 2018/07/21	2020/07/09 2020/07/10	2018/12
Tubbs Fire	2017/10/08 – 2018/02/09	2016/06/11	2018/07/25	2019/07 – 2020/10
Woolsey Fire	2018/11/08 – 2019/01/04	2018/07/22	2020/05/15 2020/05/22 2020/05/24	2018/04 – 2019/04

Table 2: Esri CNN Model Pre- and Post-Fire Accuracies

Esri convolutional neural network (CNN) model pre-fire and post-fire accuracy for the % of building correctly identified in the interface and intermix wildland-urban interface (WUI) across the Camp Fire, Tubbs Fire, and Woolsey Fire perimeters. A correctly identified building was correctly detected in the pre-fire or post-fire image (destroyed or not). Accuracies are reported for the subsets of the stratified random sample accuracy assessment on our post-classification change detection. The Camp Fire, Tubbs Fire, and Woolsey Fire have 772, 441, and 709 samples respectively.

[next page]

Esri CNN Model Pre- and Post-Fire Accuracy (%)	All Buildings, Any Tree Cover	All Buildings, < 50% Tree Cover	Major Buildings Only, Any Tree Cover	Major Buildings Only, < 50% Tree Cover
Camp Fire				
Intermix	48%	71%	56%	78%
Interface	54%	68%	65%	76%
Tubbs Fire				
Intermix	37%	51%	48%	62%
Interface	83%	84%	87%	86%
Woolsey Fire				
Intermix	41%	50%	48%	53%
Interface	61%	66%	71%	72%

Table 3: Overall accuracy, errors of omission, and errors of commission

Pre- and post-fire overall accuracy, errors of omission, and errors of commission for the Esri convolutional neural network (CNN) model.

[next page]

	Intermix		Interface	
	Pre-Fire	*Post-Fire*	*Pre-Fire*	*Post-Fire*
	Errors of Commission			
Camp	1%	2%	0%	2%
Tubbs	4%	2%	0%	0%
Woolsey	4%	3%	1%	2%
	Errors of Omission			
Camp	49%	5%	40%	10%
Tubbs	58%	18%	10%	10%
Woolsey	50%	27%	31%	25%
	Overall Accuracy			
Camp	51%	93%	60%	90%
Tubbs	42%	82%	90%	90%
Woolsey	50%	73%	69%	75%

Table 4: Spatial logistic regression model

Summary table for the spatial logistic regression model. Coefficients are the log odds ratio of destruction.

Tree Cover	Coefficients (Log Odds Ratio)	P-Value
None vs Full	-2.31	<< 1
Partial vs Full	-1.30	<< 1

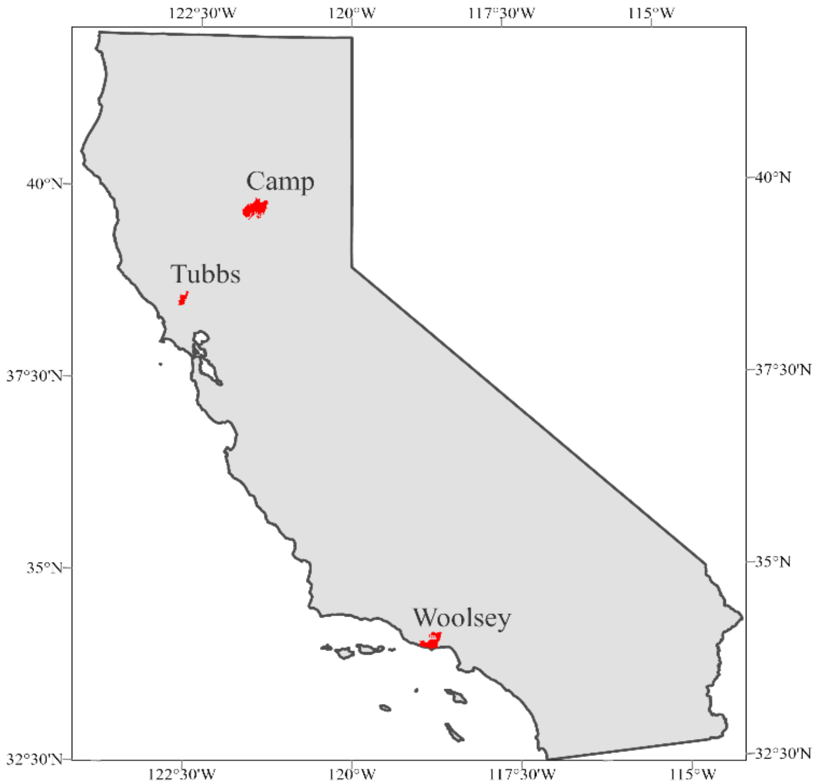

Figure 1: Overview map of the fires of interest.

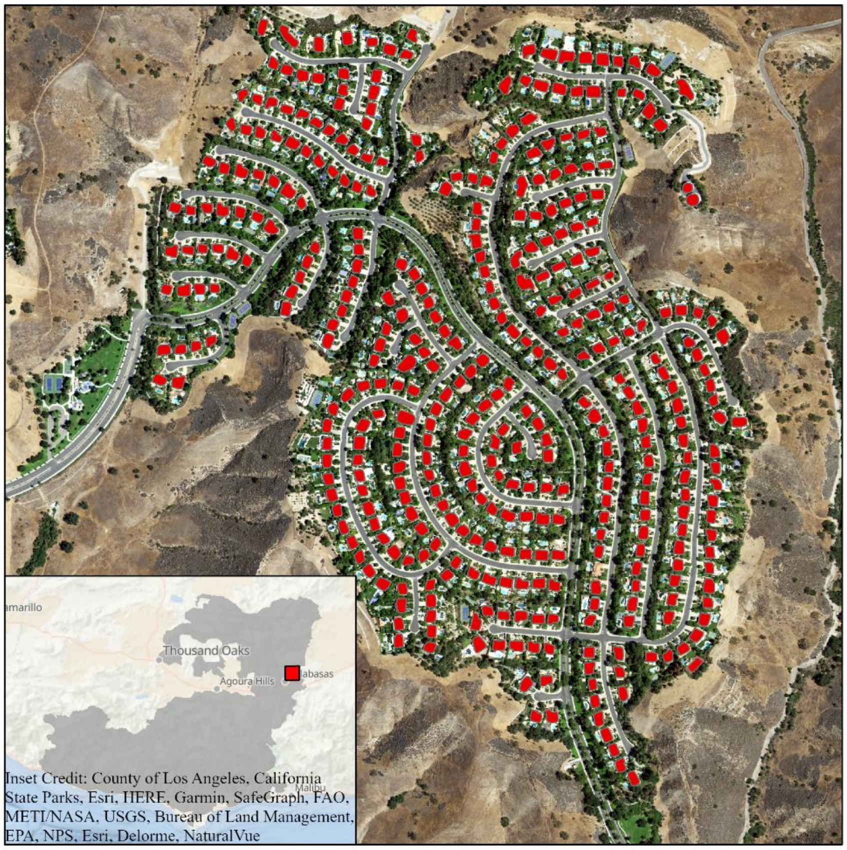

Figure 2: Detected pre-fire building footprints from the Esri convolutional neural network (CNN) model within a portion of the Woolsey Fire perimeter in Calabasas, California. Building footprints are overlaid on National Agriculture Imagery Program (NAIP) acquired pre-Woolsey Fire.

Figure 3: During our accuracy assessment, we compared the Microsoft building dataset and the Esri convolutional neural network (CNN) model results to the CAL FIRE dataset. We converted the building polygons from the Esri CNN model to point data. In our pre-fire image (above), we looked at every building to verify the Esri CNN properly detected a building. In our post-fire image (below), we looked at every destroyed building to verify that the Esri CNN model did not detect a building. For buildings that were not destroyed, we looked to see if the Esri CNN model detected a building. We then verified building destruction with the CAL FIRE dataset to see which buildings had been destroyed and not destroyed. Lastly, we checked to see if the Microsoft building dataset detected a building in the post-fire imagery.

Figure 4: Tree cover is detrimental to the Microsoft dataset and the Esri convolutional neural network (CNN) model accuracies as seen in the area near Paradise, California, where the Camp Fire was. The NAIP imagery is pre-fire.

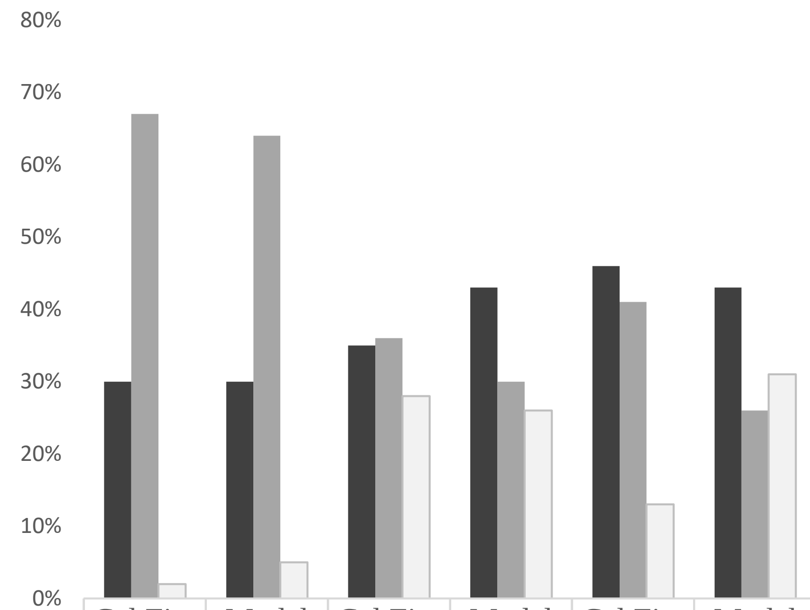

	Camp Fire		Tubbs Fire		Woolsey Fire	
	Cal Fire	Model	Cal Fire	Model	Cal Fire	Model
Interface	30%	30%	35%	43%	46%	43%
Intermix	67%	64%	36%	30%	41%	26%
Not-WUI	2%	5%	28%	26%	13%	31%

Figure 5: Esri convolutional neural network (CNN) model and CAL FIRE estimation for where buildings were destroyed when looking at destroyed buildings only.

Appendix A. Esri CNN Model Arguments

The model has five main arguments: (1) padding, (2) batch size, (3) threshold, (4) return bounding boxes, and (5) tile size.

The padding is the bordering area where the model discards detections. Changing the padding will ultimately change the stride, the amount of movement over each image. We kept the default value of 128 for all three fires.

The batch size indicates the number of image tiles the GPU will process at one time during inferencing. Inferencing refers to the process where a trained model, such as the one used here, makes predictions against new data. The model default is four. The batch size may be limited by GPU memory. The GPU we used ran out of memory with a batch size of four, so we applied a batch size of two for all three fires.

The model outputs a level of confidence for each building prediction, and the threshold assigns the minimum level of confidence the model output must have. For example, if the threshold is set to 0.6, a building is detected only if the model is at least 60% confident the feature is a building. Threshold was the most influential argument, varying for each fire and each year. Once all the other parameters were set, we found that the default of 0.9 was too high for each fire and year. We adjusted the value in increments of .05 at first until we started getting high levels of detection and then adjusted in increments of 0.01 until we found a threshold with the highest accuracy. We found that a building foundation is sometimes left behind after a building is destroyed by a fire, and the foundation sometimes appears like an intact building in aerial imagery. To prevent false detections of destroyed building foundations, the threshold was made higher post-fire.

The return bounding boxes parameter is either True or False. If set to True, a bounding box is returned around the building. Since we were interested in the buildings only and not the bounding boxes, we kept the default value, False.

For tile size, we used the default value of 512. Adjusting the tile size did not noticeably improve the model results.

Chapter 2: Mapping the wildland-urban interface for the 1970s to study decadal change using Hexagon spy satellite imagery

Contributors: Neda K. Kasraee[1,*] Afag Rizayeva[1], Mihai D. Nita[2], Volker C. Radeloff[1]

[1] SILVIS Lab, Department of Forest and Wildlife Ecology, University of Wisconsin-Madison, 1630 Linden Drive, Madison WI 53706, USA.

[2] Department of Forest Engineering, Faculty of Silviculture and Forest Engineering, Transylvania University of Brasov, 1 Sirul Beethoven, Brasov 500123, Romania.

Abstract

The wildland-urban interface (WUI), the area where the built environment intermixes or intermingles with wildland vegetation, has grown over the last several decades globally. Mapping WUI growth can be informative to land managers and policymakers, because the WUI is where many land management conflicts occur, such as human-wildlife conflicts, habitat fragmentation, and wildfires. However, WUI maps require two key pieces of information – building density and land cover. Building density and land cover information are often difficult to acquire, especially pre-1990s when global, high-resolution imagery was limited. Our goal was to test the use of the historical spy satellite Hexagon to extract building and land cover information and map the WUI. We used convolutional neural networks (CNNs) to extract building locations and an object-oriented classification to extract land cover data for the 1970s for two study areas, one in Southern California, United States and the other in New South Wales, Australia. We also created present-day WUI maps for comparison using the Microsoft building footprint dataset (updated in the late 2010s, early 2020s) for the Australia and US study areas. For the land cover datasets, we used the National Land Cover Database (updated 2019) for our US study area and European Space Agency WorldCover dataset (updated 2020) for our Australia study area. In our US study area, the WUI covered 49% in 1973, and in our Australia study area, the WUI covered 6% in 1976. The WUI grew by 7 percentage points in our US study area, and in our Australia study area, the WUI grew by 34 percentage points. In our US study area, the interface WUI grew faster than the intermix WUI while the opposite was true in our Australia study area, where only the intermix grew in size. Overall, we found that our final WUI maps had high accuracies for mapping the WUI area. We visually inspected 100 randomly placed circular sample areas, and found that 94 samples and 100 samples in the US and Australia study areas, respectively, had the correct WUI classification. Our results demonstrate that the historical spy satellite Hexagon can provide valuable information for the 1970s. With CNNs and object-oriented classification methods, we can derive building and land cover information from historical spy satellite imagery and map the WUI accurately for the 1970s.

Keywords

panchromatic satellite imagery, spy satellites, land cover mapping, object-oriented analysis, convolutional neural networks

Introduction

The wildland-urban interface (WUI), the area where buildings intermix or intermingle with wildland vegetation, is a central location for human-environmental conflicts. The WUI is especially at-risk of wildfires partly because wildfire ignitions are concentrated here (Keeley and Fotheringham, 2003; Syphard et al., 2007), and in the US, human-caused ignitions disproportionally threaten residential homes (Mietkiewicz et al., 2020). The WUI is also where wildfires destroy the most buildings (Caggiano et al., 2020; Kramer et al., 2018). With housing developments near wildland vegetation and subsequent WUI growth, there is also increased habitat fragmentation and loss (Bar-Massada et al., 2014; Gonzalez-Abraham et al., 2007; Zhang et al., 2008). Additionally, WUI growth increases the introduction and spread of invasive species, pollutants from nearby settlements and roads, and disease transfer (Bar-Massada et al., 2014). Despite the many consequences of WUI growth, the WUI is projected to continue growing, and in the contiguous US, it is the fastest-growing land use type from 2000-2010 (Radeloff et al., 2018). However, it is difficult to map the WUI prior to the 1990s due to the lack of available data. The historical spy satellite Hexagon may be used to map the WUI for the 1970s and to study WUI growth over the last half a century.

WUI maps essentially require two key pieces of information: building density data and land cover data, particularly wildland vegetation information. The WUI has been mapped for many regions including the US (Radeloff et al., 2018), south-central Chile (Miranda et al., 2020), Central Argentina (Argañaraz et al., 2017), the Polish Carpathians (Kaim et al., 2018), Italy (D'Este et al., 2021), and Lebanon (Mhawej et al., 2017). The WUI is defined using minimum thresholds of buildings density, vegetation cover, and vegetation proximity (Stewart et al., 2007). Thresholds for the intermix WUI, the area where buildings and wildland vegetation intermingle, and the interface WUI, the area where buildings are adjacent to wildland vegetation, sometimes differ (Radeloff et al., 2005). In Central Argentina, the WUI was mapped by hand digitizing 276,700 buildings and using satellite imagery to derive vegetation information (Argañaraz et al., 2017). In the US, WUI maps have been made either using decadal Census block data and the National Land Cover Database (NLCD) (Radeloff et al., 2005; 2018), or from a point-based building dataset from Microsoft and NLCD for more spatially precise WUI maps (Bar-Massada, 2021; Carlson et al., 2022). However, WUI maps are not available before the 1990s, and generally, building density and land cover data are sparse for the past, especially before 30-m Landsat satellite data became available in the mid-1980s.

Fortunately, declassified US spy satellites provide high-resolution spatial data as early as the 1960s and '70s and may potentially be used to extract important building density and land cover information and to map the WUI. The US National Reconnaissance Office launched a series of reconnaissance missions during the Cold War, and in 1971, the United States launched Hexagon to acquire high-resolution panchromatic imagery (Burnett, 2012). Hexagon was launched by the US military for reconnaissance, which means that it has high-resolution and near-global coverage for the 1970-80s. Hexagon is available in 2 - 4 feet resolution and 20 - 30 feet resolution and select areas have color infrared imagery available at 2 - 4 feet resolution. Hexagon was declassified in 2011, and while Hexagon has been used occasionally for non-military applications such as glaciology (Holzer et al., 2015; Pieczonka et al., 2013; Zhou et al., 2018), seismology (Zhou et al., 2022), and archaeology (Fowler, 2004), to our knowledge, Hexagon is largely unexploited for land use change studies and has not been used to study WUI growth.

The WUI has grown because people seek access to natural amenities and ecosystems services (Radeloff et al., 2018). In the US, WUI growth is largely due to new development when people move towards more rural areas within or adjacent to wildland vegetation (Hammer et al., 2009), and the WUI area grew by 33% from 1990 to 2010 (Radeloff et al., 2018). In Patagonia, Argentina, the WUI area grew by 76% from 1981 to 2016, with tourism being an important driver behind housing development (Godoy et al., 2019). In Spain, building development near existing urban areas and the growth of wildland vegetation in abandoned agricultural farms and silvopastures have led to WUI growth (Navarro-Carrión et al., 2021). However, WUI area growth can also be caused by regrowth in forests. In the Polish Carpathians, both an increase in new buildings and forest cover were responsible for about 13-21% of WUI area growth from 1860 to 2013 (Kaim et al., 2018). Identifying the reasons for growth in a given area may provide valuable insights into how to limit future WUI growth.

We analyzed Hexagon spy satellite imagery to extract building locations with CNNs, and land cover data with an object-oriented classification approach in order to create 1970s WUI maps for our US study area and Australia study area. Furthermore, we compared the 1970s WUI maps to the present-day (late 2010s, early 2020s) WUI maps, which we created with current building and land cover datasets. Our research questions are: (1) Can we use historical satellite imagery from Hexagon to extract building data with CNNs and land cover data with an object-oriented classification approach to accurately map the WUI? (2) Has there been WUI growth or reduction in our study areas, and if so, what are the major reasons for WUI change?

Methods

Study area

Our two study areas are in Southern California, United States (~880 km^2) and New South Wales, Australia (~1,100 km^2). Both the US and Australia study areas have experienced destructive and deadly wildfire seasons. Our US study area is located in Southern California, in San Diego County. Our Australia study area is in New South Wales, roughly 50 km northwest of Sydney and near Blue Mountains National Park. We selected these areas because they have experienced increased wildfires and housing development growth. In addition, these areas had mostly cloud-free Hexagon imagery available.

Our study area in the US was where three destructive wildfires occurred: the Cedar Fire (2003), the Witch Fire (2007), and the Cocos Fire (2014). The Cedar Fire destroyed 3,021 structures and burned about 111,000 hectares, the Witch Fire destroyed 1,711 structures and burned about 80,000 hectares, and the Cocos Fire destroyed 40 buildings and burned about 800 hectares (CAL FIRE, 2003; 2007; 2014). The Australia study area is where the Gospers Mountain Fire occurred, which was the largest recorded wildfire in New South Wales, burning more than 51,000 hectares (Boer et al., 2020; Krogh et al., 2022) and destroying 90 homes (Australian Disaster Resilience Knowledge Hub).

Data

Microsoft has mapped building footprints across the globe. Microsoft derives building footprint data from high-resolution satellite imagery using Deep Neural Networks and ResNet-34 with RefineNet up-sampling layers. We used the Microsoft building footprints to map the present-day WUI for both study areas. According to Microsoft's reported overall classification accuracies, the United States building dataset has accuracies of 98.5% precision and 92.4% recall (Microsoft, 2020), and the Australia dataset of 98.6% precision and 65% recall (Microsoft, 2020).

We analyzed Hexagon imagery to extract building and land cover information for the 1970s. We acquired Hexagon imagery via the United States Geological Survey's (USGS) Earth Explorer (https://earthexplorer.usgs.gov) at 0.95 m resolution. We selected Hexagon images based on which had the best coverage and least amount of clouds for our study area.

We rectified each scanned Hexagon image based on Structure from Motion (SfM) algorithms implemented in AgiSoft Photoscan™ (Munteanu et al., 2020; Nita et al., 2018; Rendenieks et al., 2020). Nita et al. (2018) developed our rectification approach. Hexagon imagery is available in stereoscopic coverage based on a forward and backward-facing camera. We georectified 3 scanned images for our US study area and four scanned images for our Australia study area (Table 1Table 5) by co-aligning them to generate a point-cloud, and then coordinates were assigned to the point cloud to generate orthophotos. Ultimately, we had one forward and one backward orthorectified image for each study area.

To assess present-day land cover, we used the National Land Cover Database (NLCD) dataset for California and the European Space Agency (ESA) World Cover dataset for Australia. NLCD is based on 2019 Landsat 8 imagery and has a 30-m resolution (Dewitz, 2021) while ESA WorldCover is based on 2020 Sentinel-1 and -2 imagery and has a 10-m resolution (Zanaga et al., 2021). We used NLCD instead of ESA WorldCover for our US study area because we found in our initial visual assessment that NLCD detected wildland vegetation better than ESA WorldCover.

Extracting Building Data

To extract building information from Hexagon imagery, we created a building detection CNN model within the Esri ArcPro software. We created two CNN models, one for each study area. We used the PyTorch framework using the Mask Region-based CNN (Mask R-CNN) (He et al., 2018) architecture and a ResNet-50 backbone model. When we created the training datasets and trained the models, we only used the backward Hexagon image and not the forward image for both study areas. We found using only the backward image produced the best results, as buildings were brighter and more visible than the forward image. To create training data, we hand-digitized buildings in the backward Hexagon imagery. To assess how many training samples were necessary, we trained the Mask R-CNN models in increments of 150-500 buildings at a time and monitored improvements in the model precision. Once the model precision stopped improving, we stopped adding training data. Our training dataset for our US study area had 3017 buildings, and our Australia study area had 750 buildings. For both models, we set aside 15% of the training data as validation. Our final model for the US study area had an average precision of 64% and our final model for Australia had an average precision score of 67%. Ultimately, our CNN model delineated building footprints. We converted these polygons to point data using the centroid of each polygon.

Extracting Land Cover from Hexagon

To extract land cover data from Hexagon for our two study areas, we used the approach developed in (Rizayeva et. al, unpubl.). This approach works entirely in Google Earth Engine. First, we performed segmentation to identify objects in the imagery. For this, we applied the Simple Non-Iterative Clustering (SNIC) segmentation algorithm (Achanta and Susstrunk, 2017). After testing various segmentation parameters, we selected parameters that yielded the optimal results without running out of user memory in Google Earth Engine, while ensuring that segments encompassed objects correctly. We used a segment size of 4 for California and 20 for Australia. We separated our segments into two categories after visual inspection: pure (100% of each segment has one land cover class) and mixed (more than one land cover class in each segment).

For each segment, we calculated the mean greyness level, area, perimeter, width, height, and shape (Nghi and Mai, 2008), as well as texture metrics. We selected texture metrics that emphasized intra-class variability (Farwell et al., 2021). We applied a 7x7 pixel moving window within each segment (Conners et al.,1984) and calculated object-based first-order metric standard deviation and second-order metrics entropy, homogeneity, and angular second moment. After, we applied a 10-fold Random Forest classification with majority voting (Cui et al., 2018) (.smileRandomForest) with a tree size of 100.

We analyzed both the forward and backward Hexagon images when digitizing the training and validation data. In tests, combining both images produced higher classification accuracy than using just the forward or backward image separately. To collect our training and validation data, we created a point grid across our study area with 2 km spacing. In total, we had 236 points for our US study area and 277 points for our Australia study area. For each point, we visually inspected the Hexagon imagery and labeled each point according to one of five classes: forest, scrub, agriculture, urban, and open water. We used the open water class to mask out non-buildable areas and the forest and scrub class to identify areas of wildland vegetation.

For our accuracy assessment of the land cover classification, we used a ShuffleSplit Cross-Validation. We randomly selected 80% of points within pure segments for training and the other 20% of the points were used for validation. Also in our validation dataset, we randomly selected 20% of points within the mixed segments. This random selection was repeated ten times, and we randomly selected from the entire dataset for each iteration so values selected for one iteration could have potentially been selected again for other iterations. Lastly, we averaged the accuracies of the ten resulting classifications.

Creating the Final WUI Maps

We created four WUI maps (Figure 6): 1) 1976 WUI map for our Australia study area, 2) present-day WUI map for our Australia study area, 3) 1973 WUI map for our US study area, and 4) present-day WUI map for our US study area.

We created our WUI maps based on the WUI definitions from the US Federal Register (USDA & USDI, 2001). The intermix WUI is an area where housing density exceeds 6.17 houses/km^2 and has ≥ 50% wildland vegetation. The interface WUI is defined as an area where housing density exceeds 6.17 houses/km^2 and has < 50% wildland vegetation but housing density is within 2.4 km of a wildland vegetation patch area of ≥ 5 km^2.

To map the WUI, we used a circular moving window algorithm (Bar-Massada et al., 2013) implemented in Python using the ArcPy library (Esri, 2019). Our WUI mapping algorithm required three key pieces of information: areas of open water, building information, and wildland vegetation information. We used our CNN model results for the 1970s building locations and the Microsoft dataset for our present-day building locations. Subsequently, we divided our land cover into wildland vegetation (forest, scrub), open water, and developed, or non-wildland vegetation (urban, agriculture). We did not use the urban and agriculture classes and only used the forest, scrub, and open water classes from our land cover datasets for our final WUI maps.

Using the circular window algorithm, we classified every pixel in our study area using a circular window size of 500 m. We used this window size because this is the optimal size for providing enough spatial detail without mapping isolated buildings as WUI (Carlson et al., 2022; Kaim et al., unpubl). For our first step, we found the number of building centroids and the proportion of wildland vegetation within the 500 m window. Pixels with ≥ 6.17 buildings/km^2 and ≥ 50% wildland vegetation were classified as intermix WUI. Then, for all pixels not classified as intermix WUI, we mapped those that were interface WUI. We defined proximity as areas within a 2.4 km buffer around the large wildland vegetation patches. Pixels with ≥ 6.17 buildings/km^2 that overlapped with the 2.4 km wildland vegetation buffer were classified as interface WUI.

Accuracy Assessment

To assess the accuracy of our WUI maps, we checked their accuracy based on the CNN model output, the Microsoft building dataset, the object-oriented land cover classification, and the present-day land cover data (ESA and NLCD). For each study area, we randomly placed non-overlapping circular sample areas with a radius of 500 m over our entire study area. We looked at 100 samples in our US study area and 100 samples in our Australia study area. We visually inspected each WUI map. For our 1970s WUI maps, we first counted the number of buildings in the Hexagon imagery and compared this value to how many buildings the CNN model detected. Then, we visually estimated whether there was ≥ 50% or < 50% wildland vegetation within each sample and compared that to what the object-oriented classification found.

For our present-day WUI maps, we first counted the number of buildings in the ArcGIS Pro imagery base map (Esri, 2020) and compared that value to the number of buildings that the Microsoft building dataset detected. After, we visually estimated the percent of wildland vegetation in the present-day imagery and compared this value to either the ESA or NLCD dataset.

For both our 1970s and present-day accuracy assessment, we visually inspected each sample and noted whether the WUI class was correctly classified as either intermix WUI, interface WUI, or not-WUI. In our final step, we visually inspected whether the CNN model output, Microsoft building dataset, object-oriented classification, NLCD, or ESA data were incorrect, and ultimately caused a misclassification of the WUI. Overall, we calculated errors of omission and errors of commission for our CNN model output and Microsoft building data. We also calculated overall WUI map accuracy.

Results

Land Cover from Hexagon

Our land cover maps derived from Hexagon imagery had an overall accuracy of 80±3% for our US study area, and 77±4% for our Australia study area. Overall, we found that the object-oriented classifications applied on Hexagon imagery yielded good results and allowed for accurate WUI mapping. In the 1970s, our US study area contained 85% wildland vegetation while our Australia study area contained 95% wildland vegetation. However, from 1973 to the present-day, 34% of wildland vegetation in our US study area transitioned to developed land cover. Additionally, we found that 64% of our US study area and 96% of our Australia study area experienced no land cover change.

We found that our present-day land cover map for our Australia study area was not entirely accurate due to the way ESA mapped wildland vegetation and urban areas (Figure 7), and this made it difficult to compare land cover change over time. Our 1970s WUI map used an object-oriented classification approach and ultimately mapped general urban areas. However, the ESA dataset mapped individual buildings (Figure 7) causing ESA to somewhat over classify wildland vegetation and under classify urban areas. Thus, the observed increase in wildland vegetation was largely due to differences in land cover mapping data sources and methods (Table 6). The ESA dataset is pixel-based and developed using Sentinel 1 and 2 imagery (10 m resolution), while NLCD is based on Landsat (30 m resolution). Applying the object-based classification on present-day high-resolution imagery would have yielded a present-day object-based land cover map that would have made for a true comparison of WUI change.

Buildings

Our CNN model detected buildings with high accuracy for our US study area, and we found our CNN model produced an overall accuracy of 80%, detecting 3248 buildings out of the 4078 total buildings we checked during our accuracy assessment. There were 2% commission errors and 20% omission errors (Table 8). For the Microsoft dataset, we checked 11893 buildings, and of those, 2% were commission errors and 4% were omission errors (Table 8). The Microsoft dataset had an overall accuracy of 96%. According to the CNN model and the Microsoft dataset, the number of buildings increased by over 250% (Table 7).

For our Australia study area, we found that the CNN model produced much lower accuracies. Our CNN model had an overall accuracy of 60%, detecting 61 buildings out of the 102 total buildings we checked during our accuracy assessment. We found 36% commission errors and 40% omission errors (Table 8). The Microsoft data had an overall accuracy of 89%, detecting 978 buildings of the 1096 buildings we checked. The Microsoft dataset had 4% commission errors and 11% omission errors (Table 8). The number of building according to the CNN model and Microsoft building dataset increased by about 940% (Table 7).

Ultimately, we found during our accuracy assessment that although our CNN model had low accuracies and high commission and omission errors, the final WUI map was still accurate because the 6.17 buildings/km^2 threshold was clearly met or not met.

Decadal WUI Growth

When comparing our 1970s and present-day WUI maps, we found WUI growth in both of our study areas (Table 6, Figure 8, Figure 9). In our US study area, the WUI grew overall by 7 percentage points, and building development was solely responsible for that growth. There was an especially strong increase in interface WUI, which grew by 24 percentage points. Meanwhile, the intermix WUI decreased from 42% coverage in 1973 to 25% coverage in the present-day, and this was mainly caused by new development replacing wildland vegetation, which turned formerly intermix WUI into not-WUI (Figure 10). Also, in some areas, intermix WUI changed to interface WUI (198 km^2, 23% of total study area), but there were no instances where the interface WUI turned into intermix WUI. About 47% of the study area had the same WUI classification (intermix, interface, not-WUI). Additionally, we found new WUI areas formed due to new development in areas that were originally wildland vegetation in 1973. About 19% of the total study area that was not-WUI in 1973 turned into WUI. Finally, overall WUI loss (12% of the total study area), primarily in the intermix WUI, was caused by new building development and wildland vegetation reduction, making these areas too urban to be defined as WUI.

In our Australia study area, the WUI grew by 32 percentage points, and this was entirely attributed to new building construction, not changes in wildland vegetation. The interface WUI covered just <1% of the study area in 1976, but in the present-day, there is none.

Meanwhile, the intermix WUI grew by 35 percentage points, and the new intermix WUI was almost entirely in areas that were not-WUI in 1976. About 76% of the entire study area experienced no change in WUI type while about 24% of areas that were not-WUI in 1976 turned into intermix WUI in the present-day. We generally found no areas of WUI loss.

WUI accuracy assessment

For our accuracy assessment, we checked the WUI classification for 100 randomly placed circular sample areas for each study area. When looking at WUI classification only, all 100 samples in the 1976 Australia study area WUI Map had the correct WUI classification, and 94 of the 100 samples in the 1973 US study area WUI map had the correct WUI classification. The 6 samples that did not have the correct WUI classification in the US study area were solely due to the land cover data we derived from Hexagon with our object-oriented classification. Our object-oriented classification classified some areas that were agriculture as wildland vegetation, and this caused areas to be defined as intermix WUI instead of interface WUI. However, the WUI was correctly identified, but the WUI type was incorrect. Additionally, there were areas that occasionally had incorrect WUI classifications in our final WUI maps; however, the randomly placed circular samples were not placed there. Although it was minor overall, in these areas with incorrect WUI classifications, the CNN model detected bare rock as buildings and therefore, the WUI was incorrectly detected.

For our present-day WUI maps, we found that all 100 samples had the correct WUI classification for both the US and Australia study areas. Although there were issues with the ESA dataset overdetecting wildland vegetation and underdetecting urban areas, this did not influence the final WUI classifications. The ESA dataset was pixel-based but our 1970s land cover maps were object-based. If we had applied the same object-based classification approach for the present-day using present-day high-resolution imagery, there would have been a true comparison of WUI growth over the last 50 years in both our study areas.

Discussion

We extracted land cover and building information for the 1970s from the historical spy satellite Hexagon. This allowed us to create 1970s WUI maps, which we compared to current-day WUI maps to study decadal change. We used CNNs to identify buildings, and we applied an object-oriented classification to derive land cover data from Hexagon imagery. When visually inspecting randomly placed circular sample areas, we found that our WUI maps were highly accurate (≥ 94%) for mapping the intermix and interface WUI. However, when visually inspecting the samples, both 1970s WUI maps had no misclassifications for mapping combined WUI (interface and intermix) vs. non-WUI categories. We found that the major driver of WUI growth was new building construction, and in our US study area, some areas that were WUI in the 1970s became not-WUI after new developments made the area too urban to be classified as WUI. In summary, we demonstrate that it is possible to map the WUI for the 1970s by deriving building data with CNNs and land cover data with an object-oriented classification from Hexagon imagery.

Spy satellite imagery, such as Hexagon, is especially useful for understanding change over time. High-resolution satellite data is not easily available, especially globally, pre-21st Century (Poli and Toutin, 2012). Analyses requiring high-resolution data, like WUI mapping, may use spy satellite imagery as a reference point as it is available three to four decades earlier than commercial high-resolution satellites. Additionally, spy satellite data can be combined with current imagery, such as Landsat, to study long-term changes. For example, Landsat imagery has been combined with spy satellite imagery for forest change analyses along the Latvian-Russian border (Rendenieks et al., 2020). Another study used spy satellite imagery and Landsat to study land resource changes in Senegal from the 1960s – 1990s (Tappan et al., 2000). Spy satellite imagery coupled with more current datasets can add coverage by a decade or more. Unlike other historical datasets, such as orthophotos, Hexagon has near-global coverage and processes can be automated for larger study areas as a single Hexagon frame covers the ground distance of 370 nautical miles. Although we used CNNs and Hexagon imagery to study WUI growth, there are many applications where CNNs can be applied on remotely sensed data. For example, CNNs have been used to extract roads (Alshehhi et al., 2017; Yang et al., 2019), wetlands (Mahdianpari et al., 2018; Rezaee et al., 2018), and archeological sites (Caspari and Crespo, 2019; Lambers et al., 2019; Meyer-Heß et al., 2022). CNNs have also been applied to historical spy satellite data, specifically the Corona mission which predates Hexagon, to create land cover maps (Deshpande et al., 2021) and for qanat detection (qanat: underground water supply technology) (Soroush et al., 2020).

We found that our CNN model generally performed well for detecting buildings in the Hexagon imagery. The Hexagon imagery was distorted in some areas. This can occur from the orthorectification process or sometimes, there are film and scanning distortions (Dehecq et al., 2020; Maurer and Rupper, 2015). Where those distortions occurred, it was almost impossible for the CNN model to detect buildings. The distortions were mostly present in the Australia imagery, and this may have caused the high omission and commission errors. However, we found no instances in our accuracy assessment where errors in the CNN model caused a misclassification of the WUI. Building footprint datasets rely on high-resolution imagery, but so far, building footprint datasets have been based on recent imagery, and lack the information required for retrospective analysis. Hexagon imagery allows the unique opportunity to derive historical building locations that can be directly compared to the present-day building locations.

Our object-oriented classification produced generally good accuracies for detecting land cover from Hexagon imagery. Sometimes, classes were misclassified but we found this rarely influenced our final WUI maps. For example, in some instances, bare rocks and areas of bare soil were classified as urban in remote areas. The spectral signature of bare rocks and soil is sometimes similar to impervious surfaces seen in urban areas (Deng et al., 2015; Sun et al., 2016). However, the misclassification between rock and urban did not matter for the WUI classification because both are non-wildland vegetation. However, the misclassification of agriculture as wildland vegetation did occasionally influence our final WUI map. Some agriculture fields are very similar to scrublands or grasslands in the Hexagon imagery. The misclassification of agriculture fields for other classes such as grasslands is not uncommon (Weng and Lu, 2008), and also occurs in the NLCD dataset (Wardlow and Egbert, 2003). However, agriculture is considered non-wildland vegetation, while scrub is wildland vegetation, so the underdetection of agriculture may have resulted in an overdetection of wildland vegetation. That problem was not widespread but resulted in a 6% error in the US study area 1973 WUI map and no errors for our Australia 1976 WUI map.

Both our study areas experienced WUI growth with the major driver being new building development. In our US study area, we found that the interface WUI experienced the most growth, while the intermix WUI decreased in overall size; however, new intermix WUI still formed. Meanwhile, in our Australia study area, the intermix WUI experienced the most growth while the interface WUI became nonexistent. Both the intermix and interface WUI are unique in definition and present a different set of challenges when they grow. For example, during a wildfire, fire can spread from building to building in the interface WUI (Alexandre et al., 2016) while direct ignition from vegetation is more common in the intermix WUI (Kramer et al., 2019). In the US and Patagonia, more houses are located in the interface WUI while the intermix WUI occupies more area (Argañaraz et al., 2017; Kramer et al., 2019). Since both areas are unique, studying where there is interface and intermix WUI growth and reduction may be helpful, especially for wildfire management (Hammer et al., 2007).

Limitations

Imagery with occluding cloud cover was a major limitation, especially for our Australia study area where much of the available imagery was cloudy and therefore, not useable. Additionally, our Australia study area had very bright and therefore blurry urban areas, making it impossible to train a CNN model for dense urban areas, as individual buildings were not identifiable. Sometimes, when the film is overexposed in cloudy areas, urban areas appear very bright. We reduced our study area to exclude densely urban areas to ensure the CNN model produced reliable building counts.

For our vegetation classification, we used both the forward and backward-facing imagery while for the CNN model, we used just the backward-facing image. We obtained better vegetation maps using both the forward and backward-facing images to detect vegetation but sometimes there was a shift between them. This was likely due to errors in the orthorectification process.

Conclusion

By utilizing CNNs and an object-oriented classification, we were able to derive building and land cover data for the 1970s from the historical satellite Hexagon, map the WUI then, and ultimately, study decadal WUI growth. We found WUI growth occurred in both our study areas and new building development was the driver for this growth. Our results yielded above average accuracy, and we had only a few instances where the WUI was misclassified for the 1970s. Historical spy satellites provide an important opportunity to classify development and land cover change from before the era of widespread satellite imagery.

References

Achanta, R., Susstrunk, S., 2017. Superpixels and Polygons Using Simple Non-Iterative Clustering." IEEE Conference on Computer Vision and Pattern Recognition (CVPR). 4895–4904.

Alexandre, P. M., Stewart, S.I., Keuler, N.S., Clayton, M.K., Mockrin, M.H, Bar-Massada, A., Syphard, A.D., Radeloff, V.C., 2016. Factors Related to Building Loss Due to Wildfires in the Conterminous United States. Ecol. Appl. 26:2323-2338.

Alshehhi, R., Marpu, P.R., Woon, W.L., Mura, M.D., 2017. Simultaneous Extraction of Roads and Buildings in Remote Sensing Imagery with Convolutional Neural Networks. ISPRS J. Photogramm. Remote Sens. 130: 139–49.

Argañaraz, J.P., Radeloff, V.C., Bar-Massada, A., Gavier-Pizarro, G.I., Scavuzzo, C.M., Bellis, L.M., 2017. Assessing wildfire exposure in the Wildland-Urban Interface area of the mountains of central Argentina. J. Environ. Manage. 196, 499–510.

Bar-Massada, A., 2021. A Comparative Analysis of Two Major Approaches for Mapping the Wildland-Urban Interface: A Case Study in California. Land. 10, 679.

Bar-Massada, A., Radeloff, V.C., Stewart, S.I., 2014. Biotic and Abiotic Effects of Human Settlements in the Wildland–Urban Interface. BioScience. 64, 429–437.

Bar-Massada, A., Stewart, S.I., Hammer, R.B., Mockrin, M.H., Radeloff, V.C., 2013. Using Structure Locations as a Basis for Mapping the Wildland Urban Interface. J. Environ. Manage. 128: 540-547., 540–47.

Australian Disaster Resilience Knowledge Hub. Black Summer Bushfires, NSW, 2019-20.https://knowledge.aidr.org.au/resources/black-summer-bushfires-nsw-2019-20/ (accessed 31 July 2022)

Boer, M.M., Resco de Dios, V., Bradstock, R.A., 2020. Unprecedented Burn Area of Australian Mega Forest Fires. Nat. Clim. Change. 10: 171–72.

Burnett, M. G., 2012. Hexagon (KH-9) Mapping Camera Program and Evolution. Center for the Study of National Reconnaissance.

Caggiano, M. D., Hawbaker, T.J., Gannon, B.M., Hoffman, C.M., 2020. Building Loss in WUI Disasters: Evaluating the Core Components of the Wildland–Urban Interface Definition. Fire. 3: 73.

Carlson, A.R., Helmers, D.P., Hawbaker, T.J., Mockrin, M.H., Radeloff, V.C., 2022. The wildland-urban interface in the United States based on 125 million building locations. Ecol. Appl. e2597.

Caspari, G., Crespo, P., 2019. Convolutional Neural Networks for Archaeological Site Detection – Finding 'Princely' Tombs. J. Archaeol. Sci. 110: 104998.

CAL FIRE, 2003. Cedar Fire Incident Report. https://www.fire.ca.gov/incidents/2003/10/25/cedar-fire/.(accessed 3 August 2022)

CAL FIRE, 2007. Witch Fire Incident Report. https://www.fire.ca.gov/incidents/2007/10/21/witch-fire/.(accessed 3 August 2022)

CAL FIRE, 2014. Cocos Fire Incident Report. https://www.fire.ca.gov/incidents/2014/5/14/cocos-fire/.(accessed 3 August 2022)

Conners, R. W., Trivedi, M.M., Harlow, C.A., 1984. Segmentation of a High-Resolution Urban Scene Using Texture Operators. Computer Vision, Graphics, and Image Processing. 25: 273–310.

Cui, G., Lv, G., Li, G., Benediktsson, J.A., Lu, Y., 2018. Refining Land Cover Classification Maps Based on Dual-Adaptive Majority Voting Strategy for Very High Resolution Remote Sensing Images. Remote Sens. 10 (8): 1238.

Dehecq, A., Gardner, A.S., Alexandrov, O., McMichael, S., Hugonnet, R., Shean, D., Marty, M., 2020. Automated Processing of Declassified KH-9 Hexagon Satellite Images for Global Elevation Change Analysis Since the 1970s. Front. Earth Sci. 8: 516.

Deng, Y., Wu, C., Li, M., Chen, R., 2015. RNDSI: A Ratio Normalized Difference Soil Index for Remote Sensing of Urban/Suburban Environments. Int. J. Appl. Earth Obs. Geoinf. 39: 40–48.

Deshpande, P., Belwalkar, A., Dikshit, O., Tripathi, S., 2021. Historical Land Cover Classification from CORONA Imagery Using Convolutional Neural Networks and Geometric Moments. Int. J. Remote Sens. 42: 5144–71.

D'Este, M., Giannico, V., Lafortezza, R., Sanesi, G., Elia, M., 2021. The Wildland-Urban Interface Map of Italy: A Nationwide Dataset for Wildfire Risk Management. Data Brief 38: 107427.

Dewitz, J. 2021. National Land Cover Database (NLCD) 2019 Products. U.S. Geological Survey. Farwell, L.S., Gudex-Cross, D., Anise, I.E., Bosch, M.J., Olah, A.M., Radeloff, V.C., Razenkova, E., 2021. Satellite Image Texture Captures Vegetation Heterogeneity and Explains Patterns of Bird Richness. Remote Sens. Environ. 253: 112175.

Fowler, M., 2004. Archaeology through the Keyhole: The Serendipity Effect of Aerial Reconnaissance Revisited. Interdiscip. Sci. Rev. 29: 118–34.

Godoy, M.M., Martinuzzi, S., Kramer, H.A., Defossé, G.E., Argañaraz, J., Radeloff, V.C., 2019. Rapid WUI growth in a natural amenity-rich region in central-western Patagonia, Argentina. Int. J. Wildland Fire. 28, 473–484.

Gonzalez-Abraham, C. E., Radeloff, V.C., Hammer, R.B., Hawbaker, T.J., Stewart, S.I., Clayton, M.K., 2007. Building Patterns and Landscape Fragmentation in Northern Wisconsin, USA. Landscape Ecol. 22: 217–30.

Hammer, R.B., Radeloff, V.C., Fried, J.S., Stewart, S.I., 2007. Wildland–Urban Interface Housing Growth during the 1990s in California, Oregon, and Washington. Int. J. Wildland Fire. 16: 255–65.

Hammer, R.B., Stewart, S.I., Radeloff, V.C., 2009. Demographic Trends, the Wildland–Urban Interface, and Wildfire Management. Soc. Nat. Resour. 22, 777–782.

He, K., Gkioxari, G., Dollár, P., Girshick, R., 2018. Mask R-CNN. arXivLabs, Retrieved 25 April 2022, from the arXiv database.

Holzer, N., Vijay, S., Yao, T., Xu, B., Buchroithner, M., Bolch, T., 2015. Four Decades of Glacier Variations at Muztagh Ata (Eastern Pamir): A Multi-Sensor Study Including Hexagon KH-9 and Pléiades Data. The Cryosphere. 9: 2071–88.

Kaim, D., Radeloff, V.C., Szwagrzyk, M., Dobosz, M., Ostafin, K., 2018. Long-Term Changes of the Wildland–Urban Interface in the Polish Carpathians. ISPRS Int. J. Geo-Inf. 7, 137.

Keeley, J.E., Fotheringham, C.J., 2003. Impact of past, present, and future fire regimes on North American Mediterranean shrublands, in: Veblen, T.T., Baker, W.L., Montenegro, G., Swetnam, T.W. (Eds.), Fire and Climatic Change in Temperate Ecosystems of the Western Americas, Ecological Studies. Springer-Verlag, New York, pp. 218-262.

Kramer, H. A., Mockrin, M.H., Alexandre, P.M., Stewart, S.I., Radeloff, V.C., 2018. Where Wildfires Destroy Buildings in the US Relative to the Wildland–Urban Interface and National Fire Outreach Programs. Int. J. Wildland Fire. 27: 329–41.

Kramer, H., Mockrin, M., Alexandre, P., Radeloff, V., 2019. High wildfire damage in interface communities in California. Int. J. Wildland Fire 28, 641-650.

Krogh, M., Gorissen, S., Baird, I.R.C., Keith, D.A., 2022. Impacts of the Gospers Mountain Wildfire on the Flora and Fauna of Mining-Impacted Newnes Plateau Shrub Swamps in Australia's Eastern Highlands." Australian Zoologist (2022).

Lambers, K., Verschoof-van der Vaart, W.B., Bourgeois, Q.P.J., 2019. Integrating Remote Sensing, Machine Learning, and Citizen Science in Dutch Archaeological Prospection. Remote Sens. 11: 794.

Mahdianpari, M., Salehi, B., Rezaee, M., Mohammadimanesh, F., Zhang, Y., 2018. Very Deep Convolutional Neural Networks for Complex Land Cover Mapping Using Multispectral Remote Sensing Imagery. Remote Sens. 10: 1119.

Maurer, J., Rupper, S., 2015. Tapping into the Hexagon Spy Imagery Database: A New Automated Pipeline for Geomorphic Change Detection. ISPRS J. Photogramm. Remote Sens. 108: 113–27.

Meyer-Heß, M. F., Pfeffer, I., Juergens, C., 2022. Application of Convolutional Neural Networks on Digital Terrain Models for Analyzing Spatial Relations in Archaeology. Remote Sens. 14 (11): 2535.

Mhawej, M., Faour, G., Adjizian-Gerard, J., 2017. Establishing the Wildland-Urban interface building risk index (WUIBRI): The case study of Beit-Meri. Urban For. Urban Greening. 24, 175–183.

Microsoft, 2018. US Building Footprints. https://github.com/microsoft/USBuildingFootprints/ (accessed 21 April 2022).

Microsoft, 2020. Australia Building Footprints. https://github.com/microsoft/AustraliaBuildingFootprints (accessed 21 April 2022)

Mietkiewicz, N., Balch, J.K., Schoennagel, T., Leyk, S., St. Denis, L.A., Bradley, B.A., 2020. In the Line of Fire: Consequences of Human-Ignited Wildfires to Homes in the U.S. (1992– 2015). Fire. 3: 50.

Miranda, A., Carrasco, J., González, M., Pais, C., Lara, A., Altamirano, A., Weintraub, A., Syphard, A.D., 2020. Evidence-Based Mapping of the Wildland-Urban Interface to Better Identify Human Communities Threatened by Wildfires. Environ. Res. Lett. 15: 094069.

Munteanu, C., Kamp, J., Nita, M.D., Klein, N., Kraemer, B.M., Müller, D., Koshkina, A., Prishchepov, A.V., and Kuemmerle, T., 2020. Cold War Spy Satellite Images Reveal Long-Term Declines of a Philopatric Keystone Species in Response to Cropland Expansion. Proc. R. Soc. B: Biological Sciences. 287: 20192897.

Navarro-Carrión, J.T, León-Cadena, P., Ramon-Morte, A., 2021. Open Data Repositories and Geo Small Data for Mapping the Wildfire Risk Exposure in Wildland Urban Interface

(WUI) in Spain: A Case Study in the Valencian Region. Remote Sens. Appl.: Soc. Environ. 22: 100500.

Nghi, D.H., Mai, L.C., 2008. An Object-Oriented Classification Techniques for High Resolution Imagery. International Symposium on Geoinformatics for Spatial Infrastructure Development in Earth and Allied Sciences.

Nita, M.D., Munteanu, C., Gutman, G., Abrudan, I.V., Radeloff, V.C., 2018. Widespread Forest Cutting in the Aftermath of World War II Captured by Broad-Scale Historical Corona Spy Satellite Photography. Remote Sens. Environ. 204: 322–32.

Pieczonka, T., Bolch, T., Junfeng, W., Shiyin, L., 2013. Heterogeneous Mass Loss of Glaciers in the Aksu-Tarim Catchment (Central Tien Shan) Revealed by 1976 KH-9 Hexagon and 2009 SPOT-5 Stereo Imagery. Remote Sens. Environ. 130: 233–44.

Poli, D., Toutin, T., 2012. Review of Developments in Geometric Modelling for High Resolution Satellite Pushbroom Sensors. Photogramm. Rec. 27: 58–73.

Radeloff, V. C., Hammer, R. B., Stewart, S. I., Fried, J. S., Holcomb, S. S., McKeefry, J. F., 2005. The Wildland-Urban Interface in the United States. Ecol. Appl. 15:799-805

Radeloff, V.C., Helmers, D.P., Kramer, H.A., Mockrin, M.H., Alexandre, P.M., Bar-Massada, A., Butsic, V., Hawbaker, T.J., Martinuzzi, S., Syphard, A.D., Stewart, S.I., 2018. Rapid growth of the US wildland-urban interface raises wildfire risk. PNAS 115, 3314–3319.

Rendenieks, Z., Nita, M.D., Nikodemus, O., Radeloff, V.C., 2020. Half a Century of Forest Cover Change along the Latvian-Russian Border Captured by Object-Based Image Analysis of Corona and Landsat TM/OLI Data. Remote Sens. Environ. 249: 112010.

Rezaee, M., Mahdianpari, M., Zhang, Y., Salehi, B., 2018. Deep Convolutional Neural Network for Complex Wetland Classification Using Optical Remote Sensing Imagery. IEEE J. Sel. Top. Appl. Earth Obs. Remote Sens. 11: 3030–39.

Soroush, M., Mehrtash, A., Khazraee, E., Ur, J.A., 2020. Deep Learning in Archaeological Remote Sensing: Automated Qanat Detection in the Kurdistan Region of Iraq. Remote Sens. 12: 500.

Stewart, S.I., Radeloff, V.C., Hammer, R.B., Hawbaker, T.J., 2007. Defining the Wildland–Urban Interface. J. For. 105, 201–207.

Sun, G., Chen, X., Jia, X., Yao, Y., Wang, Z., 2016. Combinational Build-Up Index (CBI) for Effective Impervious Surface Mapping in Urban Areas. IEEE J. Sel. Top. Appl. Earth Obs. Remote Sens. 9: 2081–92.

Syphard, A.D., Radeloff, V.C., Keeley, J.E., Hawbaker, T.J., Clayton, M.K., Stewart, S.I., Hammer, R.B., 2007. Human Influence on California Fire Regimes. Ecol. Appl. 17, 1388–1402.

Tappan, G., Hadj, A., Wood, E., Lietzow, R.W., 2000. Use of Argon, Corona, and Landsat Imagery to Assess 30 Years of Land Resource Changes in West-Central Senegal. Photogramm. Eng. Remote Sens. 66: 727–35.

USDA, USDI, 2001. Urban wildland interface communities within vicinity of federal lands that are at high risk from wildfire. Fed Regist. 66, 751–777.

Wardlow, B.D., Egbert, S.L., 2003. A State-Level Comparative Analysis of the GAP and NLCD Land-Cover Data Sets. Photogramm. Eng. Remote Sens. 69: 1387–97.

Weng, Q., Lu, L., 2008. A Sub-Pixel Analysis of Urbanization Effect on Land Surface Temperature and Its Interplay with Impervious Surface and Vegetation Coverage in Indianapolis, United States. Int. J. Appl. Earth Obs. Geoinf. 10: 68–83.

Yang, X., Li, X., Ye, Y., Lau, R. Y. K., Zhang, X., Huang, X., 2019. Road Detection and Centerline Extraction Via Deep Recurrent Convolutional Neural Network U-Net. IEEE Trans. Geosci. Remote Sens. 57: 7209–20.

Zanaga, D., Van De Kerchove, R., De Keersmaecker, W., Souverijns, N., Brockmann, C., Quast, R., Wevers, J., Grosu, A., Paccini, A., Vergnaud, S., Cartus, O., Santoro, M., Fritz, S., Georgieva, I., Lesiv, M., Carter, S., Herold, M., Li, Linlin, Tsendbazar, N.E., Ramoino, F., Arino, O., 2021. ESA WorldCover 10 m 2020 v100.

Zhang, Y., He, H.S., Yang, J., 2008. The Wildland–Urban Interface Dynamics in the Southeastern U.S. from 1990 to 2000. Landscape Urban Plann. 85: 155–62.

Zhou, Y., Chen, G., Qiao, X., Lu, L., 2022. Mining High-Resolution KH-9 Panoramic Imagery to Determine Earthquake Deformation: Methods and Applications. IEEE Trans. Geosci. Remote Sens. 60: 1–12.

Zhou, Y., Li, Z., Li, J., Zhao, R., Ding, X., 2018. Glacier Mass Balance in the Qinghai–Tibet Plateau and Its Surroundings from the Mid-1970s to 2000 Based on Hexagon KH-9 and SRTM DEMs. Remote Sens. Environ. 210: 96–112.

Table 5: Hexagon images used

	Image Entity ID	Date Acquired
Southern California	D3C1207-100096A010	1973/11/20
	D3C1207-100096A011	1973/11/20
	D3C1207-100096F010	1973/11/20
New South Wales	D3C1212-400931A043	1976/11/18
	D3C1212-400931A044	1976/11/18
	D3C1212-400931F043	1976/11/18
	D3C1212-400931F044	1976/11/18

Table 6: WUI and land cover totals

The 1970s wildland-urban interface (WUI) maps were created using Hexagon imagery. The present-day WUI maps were created using building data from the Microsoft building footprint datasets for the Australia and the US. The land cover data for the present-day WUI maps were the National Land Cover Database for the US study area and the European Space Agency WorldCover dataset for the Australia study area.

Study Area	Intermix WUI	Interface WUI	Total WUI	Developed Area	Wildland Vegetation
US					
1973	42%	7%	49%	14%	85%
Present-Day	25%	31%	56%	46%	53%
Australia					
1976	5%	< 1%	6%	3%	95%
Present-Day	40%	0%	40%	< 1%	98%

Table 7: Number of Buildings

The 1970s building counts are derived from the convolutional neural network (CNN) models and Hexagon imagery, and the present-day building counts are from the Microsoft building footprint dataset.

	1970s Building Count	Present-Day Building Count
US Study Area	47,717	174,021
Australia Study Area	1,125	11,686

Table 8: Commission Errors, Omission Errors, and Overall Accuracy

The commission errors, omission errors, and overall accuracy for the 1) buildings, 2) land cover, and 3) wildland-urban interface (WUI) classification. The 1970s buildings are derived with convolutional neural networks (CNNs) and Hexagon imagery. The present-day buildings are from the Microsoft building footprint dataset. The 1970s land cover is derived using an object-oriented classification with Hexagon imagery. The present-day land cover for the US study area is from the National Land Cover Database (NCLD), and for the Australia study area, it is from the European Space Agency (ESA) WorldCover dataset. Our WUI classifications were produced using an algorithm that utilized the building and land cover data for the respective study area and year.

[next page]

	Commission Errors		Omission Errors		Overall Accuracy	
	1970s	**Present-Day**	**1970s**	**Present-Day**	**1970s**	**Present-Day**
	US Study Area					
Buildings	2%	2%	20%	4%	80%	96%
Land Cover	developed: 0% wildland veg.: 20%	developed: 0% wildland veg.: 0 %	developed: 73% wildland veg.: 0 %	developed: 0% wildland veg.: 0 %	85%	100%
WUI Classification	not-wui: 0% intermix: 13% interface: 0%	not-wui: 0% intermix: 0% interface: 0%	not-wui: 0% intermix: 0% interface: 45%	not-wui: 0% intermix: 0% interface: 0%	94%	100%
	Australia Study Area					
Buildings	36%	4%	40%	11%	60%	89%
Land Cover	developed: 0% wildland veg.: 0%	developed: 0% wildland veg.: 0%	developed: 0% wildland veg.: 0%	developed: 0% wildland veg.: 0%	100%	100%

WUI Classification	not-wui: 0% intermix: 0% interface: 0%	not-wui: 0% intermix: 0% interface: 0%	not-wui: 0% intermix: 0% interface: 0%	not-wui: 0% intermix: 0% interface: 0%	100%	100%

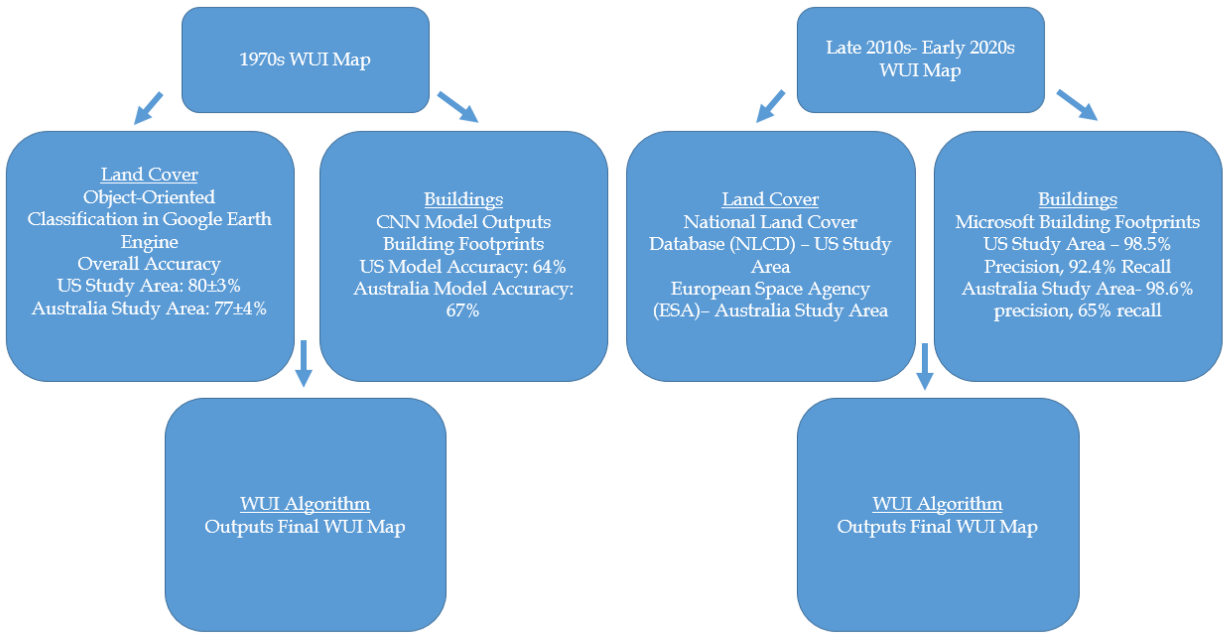

Figure 6: Flowchart showing the methods used to create the 1970s and present-day WUI maps for our US and Australia study areas.

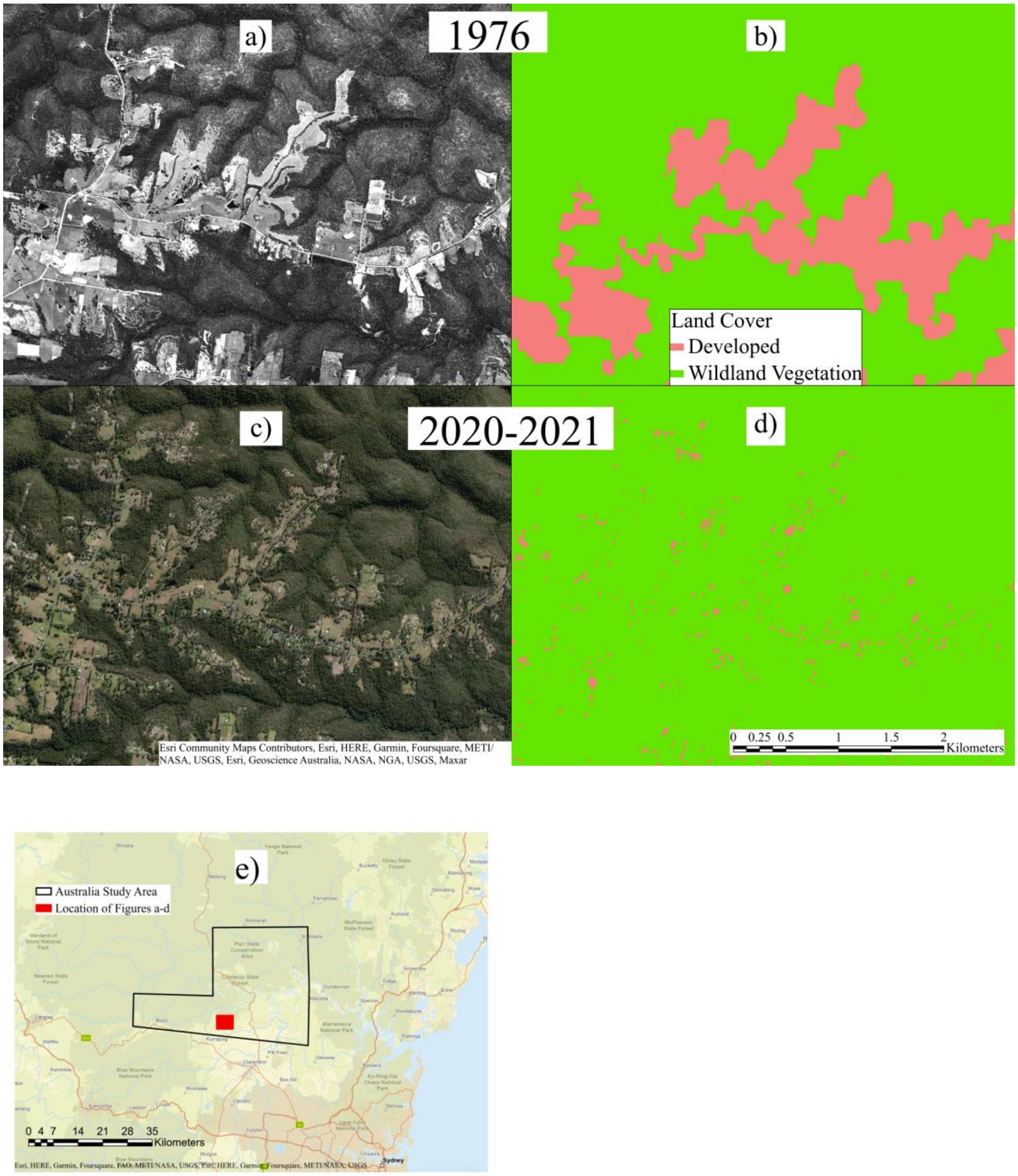

Figure 7: a) A select area of the Australia study area in 1976; b) The results of our object-oriented classification for 1976 for the selected extent. The object-oriented classification defined urban well in this example; c) The extent for 2021. The study area has had minimal to no changes since 1976; d) The ESA WorldCover dataset for 2020

for the selected extent. Even though the study area has experienced no change in land cover, ESA WorldCover has a pixel-based classification and therefore, produces a more speckled appearance. ESA WorldCover also missed a few urban areas. When comparing the two land cover datasets, it appears that there has been a reduction in developed areas; however, there has been no change; e) where the extent is located within our Australia study area.

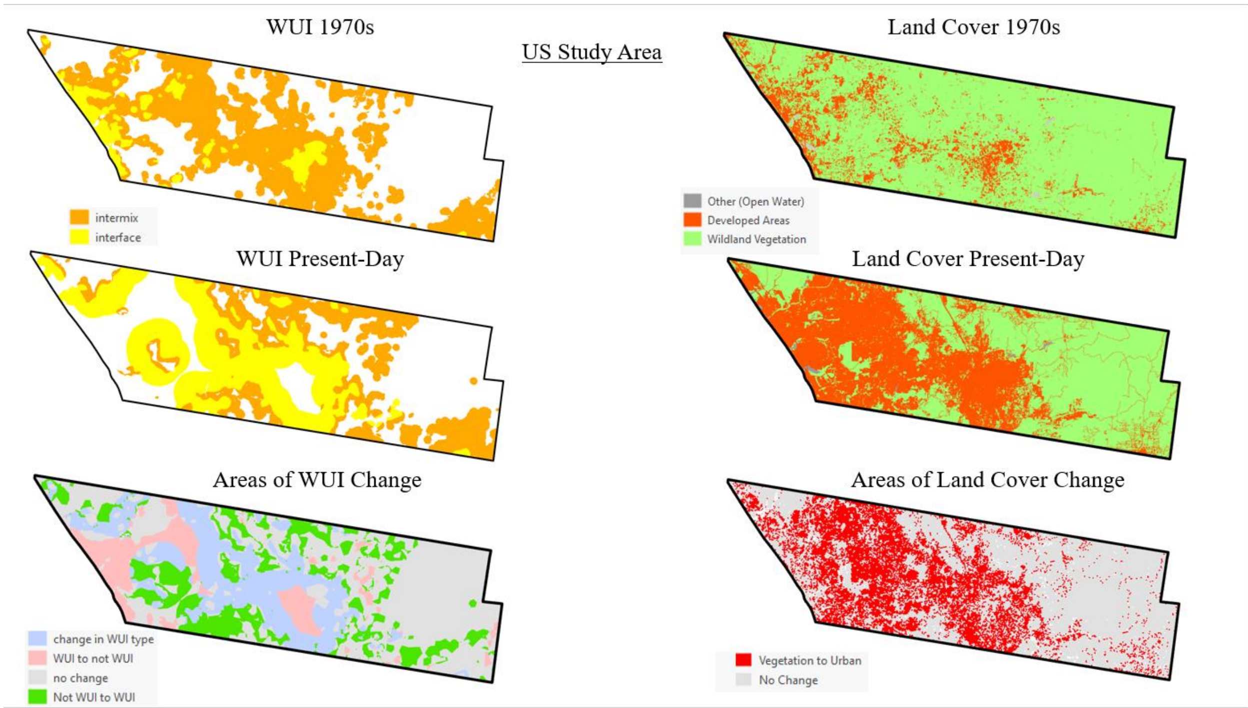

Figure 8: Changes in WUI and land cover for our US study area.

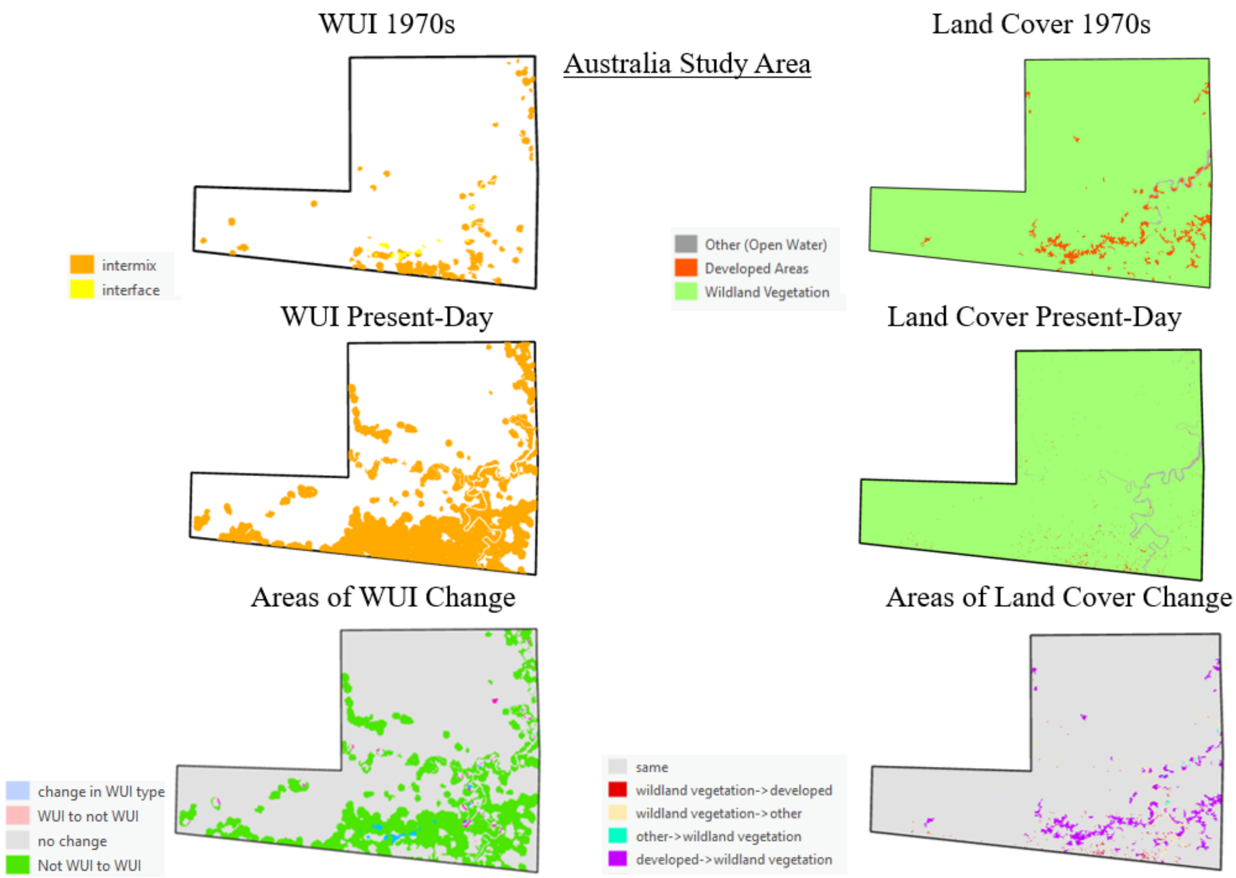

Figure 9: Changes in WUI and land cover for our Australia study area.

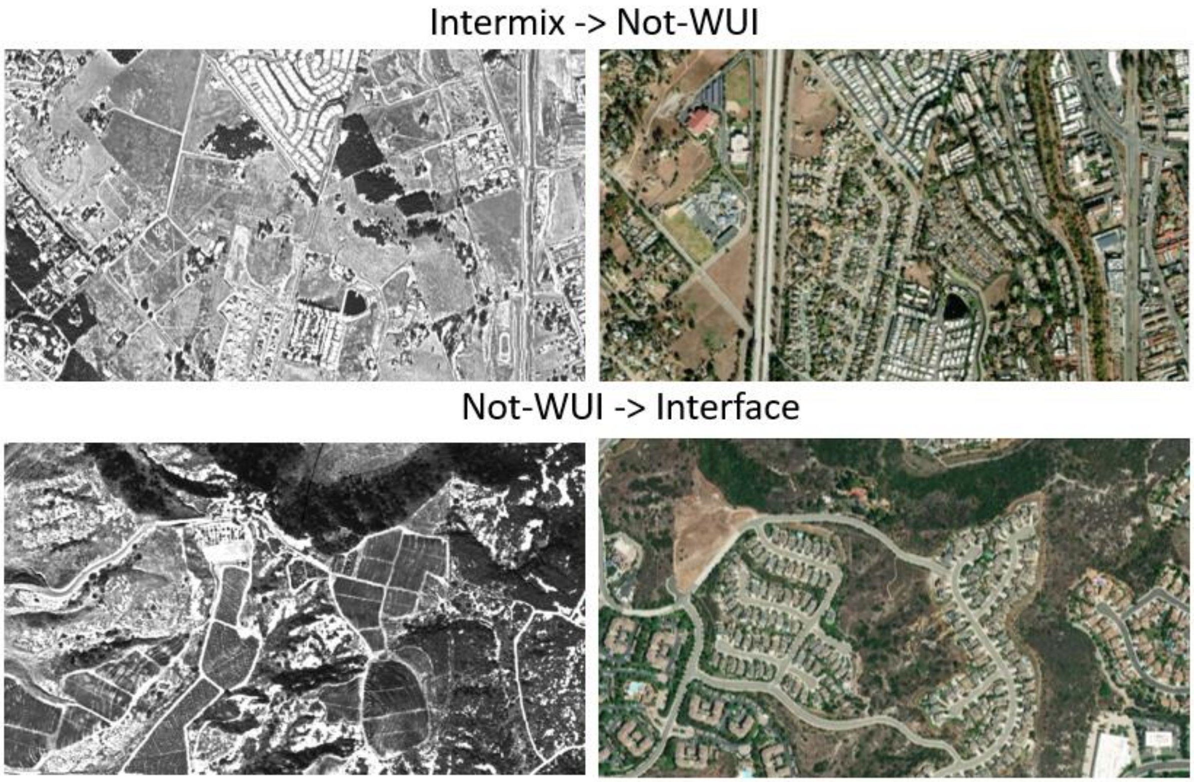

Figure 10: Examples of WUI change in our US study area. The 1973 image is from Hexagon and the present-day image is from Maxar.